ESNT workshop at Saclay on "Restoring broken symmetries within the nuclear Energy Density Functional method", September 13-15, 2011

3D angular momentum restored calculations with a nuclear covariant energy density functional

Jiang Ming Yao (尧江明)

Physique Nucléaire Théorique et Physique Mathématique,
Université Libre de Bruxelles, C.P. 229, B-1050 Bruxelles, Belgium
&
School of Physical Science and Technology,
Southwest University, Chongqing, 400715 China

September 15, 2011

ULB UNIVERSITÉ LIBRE DE BRUXELLES, UNIVERSITÉ D'EUROPE

Outline

Success of nuclear covariant density functional

- Energy density functional (EDF) theory in nuclear physics is nowadays the most important microscopic approach for large-scale nuclear structure calculations in medium and heavy nuclei. *M. Bender, P.-H. Heenen, P.-G. Reinhard, Rev. Modern Phys. 75 (2003) 121. G. A. Lalazissis, P. Ring, D. Vretenar (Eds.), Extended Density Functionals in Nuclear Structure Physics, in: Lecture Notes in Physics, vol. 641, Springer, Heidelberg, 2004.*
- In the past decades, covariant (relativistic) EDF has achieved comparable success with other non-relativistic EDFs in describing many structure properties of nuclei all over the nuclear chart, keeping some inherent advantages. *Reinhard (1989), Ring (1996), Vretenar (2005), Meng (2006), Niksic (2011)* [also shown in the talk by Dario Vretenar]

advantages in using functionals with manifest covariance

1. Natural inclusion of the nucleon spin degree of freedom
2. Nuclear spin-orbit potential emerges automatically
3. An unique parametrization of time-odd components (nuclear currents and magnetism) in nuclear mean-field
4. A distinction between scalar and four-vector nucleon selfenergies, leading to a natural saturation mechanism of nuclear matter
5. Emergence of pseudo-spin/spin symmetry in nucleon/anti-nucleon spectra

Outline

Building blocks

The basic building blocks of an effective Lagrangian density are the densities and currents bilinear in the Dirac spinor field ψ of the nucleon:

$$(\bar{\psi}\mathcal{O}\Gamma\psi), \qquad \mathcal{O} \in \{1, \vec{\tau}\}, \qquad \Gamma \in \{1, \gamma_\mu, \gamma_5, \gamma_5\gamma_\mu, \sigma_{\mu\nu}\}, \tag{1}$$

The effective Lagrangian can be written as a power series in the currents $(\bar{\psi}\mathcal{O}\Gamma\psi)$ and their derivatives, with higher-order terms representing in-medium many-body correlations. In the following, we start with the Lagrangian density of the point-coupling model, including four channels.

Four-fermion interaction terms

isoscalar – scalar: $(\bar{\psi}\psi)^2$
isoscalar – vector: $(\bar{\psi}\gamma_\mu\psi)(\bar{\psi}\gamma^\mu\psi)$
isovector – scalar: $(\bar{\psi}\vec{\tau}\psi)\cdot(\bar{\psi}\vec{\tau}\psi)$
isovector – vector: $(\bar{\psi}\vec{\tau}\gamma_\mu\psi)\cdot(\bar{\psi}\vec{\tau}\gamma^\mu\psi)$

Effective Lagrangian density

Effective Lagrangian density with higher-order self-coupling terms

$$\mathcal{L} = \mathcal{L}^{\rm free} + \mathcal{L}^{\rm 4f} + \mathcal{L}^{\rm hot} + \mathcal{L}^{\rm der} + \mathcal{L}^{\rm em},$$

where,

$$\begin{aligned}
\mathcal{L}^{\rm free} &= \bar{\psi}(i\gamma_\mu\partial^\mu - m)\psi, && \text{(2a)}\\
\mathcal{L}^{\rm 4f} &= -\frac{1}{2}[\alpha_S(\bar{\psi}\psi)(\bar{\psi}\psi) + \alpha_V(\bar{\psi}\gamma_\mu\psi)(\bar{\psi}\gamma^\mu\psi) \\
&\quad +\alpha_{TS}(\bar{\psi}\vec{\tau}\psi)\cdot(\bar{\psi}\vec{\tau}\psi) + \alpha_{TV}(\bar{\psi}\vec{\tau}\gamma_\mu\psi)\cdot(\bar{\psi}\vec{\tau}\gamma^\mu\psi)], && \text{(2b)}\\
\mathcal{L}^{\rm hot} &= -\frac{1}{3}\beta_S(\bar{\psi}\psi)^3 - \frac{1}{4}\gamma_S(\bar{\psi}\psi)^4 - \frac{1}{4}\gamma_V(\bar{\psi}\gamma_\mu\psi)^4, && \text{(2c)}\\
\mathcal{L}^{\rm der} &= -\frac{1}{2}[\delta_S\partial_\nu(\bar{\psi}\psi)\partial^\nu(\bar{\psi}\psi) + \delta_V\partial_\nu(\bar{\psi}\gamma_\mu\psi)\partial^\nu(\bar{\psi}\gamma^\mu\psi) \\
&\quad +\delta_{TS}\partial_\nu(\bar{\psi}\vec{\tau}\psi)\cdot\partial^\nu(\bar{\psi}\vec{\tau}\psi) + \delta_{TV}\partial_\nu(\bar{\psi}\vec{\tau}\gamma_\mu\psi)\cdot\partial^\nu(\bar{\psi}\vec{\tau}\gamma^\mu\psi)], && \text{(2d)}\\
\mathcal{L}^{\rm em} &= -e\bar{\psi}\gamma^\mu\frac{1-\tau_3}{2}\psi A_\mu - \frac{1}{4}F^{\mu\nu}F_{\mu\nu}. && \text{(2e)}
\end{aligned}$$

Note: There are totally 9 free parameters to be determined if we neglect the isovector-scalar channel.

Effective Lagrangian density

Effective Lagrangian density with higher-order self-coupling terms

$$\mathcal{L} = \mathcal{L}^{\rm free} + \mathcal{L}^{\rm 4f} + \mathcal{L}^{\rm hot} + \mathcal{L}^{\rm der} + \mathcal{L}^{\rm em},$$

where,

$$\mathcal{L}^{\rm free} = \bar{\psi}(i\gamma_\mu\partial^\mu - m)\psi, \tag{2a}$$

$$\mathcal{L}^{\rm 4f} = \frac{1}{2}[\alpha_S(\bar{\psi}\psi)(\bar{\psi}\psi) + \alpha_V(\bar{\psi}\gamma_\mu\psi)(\bar{\psi}\gamma^\mu\psi)$$

Remark

The non-linear coupling terms $-\frac{1}{3}\beta_S(\bar{\psi}\psi)^3 - \frac{1}{4}\gamma_S(\bar{\psi}\psi)^4$ are necessary for reproducing incompressibility and surface properties [*J. Boguta, A. R. Bodmer, NPA292(1977)413*]. Is it possible to introduce *scale-like density* in Skyrme-force to avoid the non-integer ρ^α term?

$$+\delta_{TS}\partial_\nu(\bar{\psi}\vec{\tau}\psi)\cdot\partial^\nu(\bar{\psi}\vec{\tau}\psi) + \delta_{TV}\partial_\nu(\bar{\psi}\vec{\tau}\gamma_\mu\psi)\cdot\partial^\nu(\bar{\psi}\vec{\tau}\gamma^\mu\psi)] \tag{2d}$$

$$\mathcal{L}^{\rm em} = -e\bar{\psi}\gamma^\mu\frac{1-\tau_3}{2}\psi A_\mu - \frac{1}{4}F^{\mu\nu}F_{\mu\nu}. \tag{2e}$$

Note: There are totally 9 free parameters to be determined if we neglect the isovector-scalar channel.

Energy density functional

Energy density functional

$$\mathcal{E}^{SR}_{\rm DF}[\rho_S, j_i^\mu, \kappa, \kappa^*] = \mathcal{E}^{\rm kin}[j_V^0] + \mathcal{E}^{\rm em}[j_V^0] + \mathcal{E}^{\rm int}[\rho_S, j_i^\mu] + \mathcal{E}^{\rm pair}[\kappa, \kappa^*] \tag{3}$$

kinetic part and electrostatic part

$$\mathcal{E}^{\rm kin} = {\rm Tr}[(\boldsymbol{\alpha}\cdot\mathbf{p} + \beta m)\,\rho_V], \qquad \mathcal{E}^{\rm em} = {\rm Tr}[\frac{e}{2}A^0\rho_p] \tag{4}$$

interaction part

$$\begin{aligned}\mathcal{E}^{\rm int} \;=\; {\rm Tr}\Big[&\frac{\alpha_S}{2}\rho_S^2 + \frac{\beta_S}{3}\rho_S^3 + \frac{\gamma_S}{4}\rho_S^4 + \frac{\delta_S}{2}\rho_S\triangle\rho_S + \frac{\alpha_V}{2}j_\mu j^\mu + \frac{\gamma_V}{4}(j_\mu j^\mu)^2 \\ &+ \frac{\delta_V}{2}j_\mu\triangle j^\mu + \frac{\alpha_{TV}}{2}\vec{j}^\mu_{TV}\cdot(\vec{j}_{TV})_\mu + \frac{\delta_{TV}}{2}\vec{j}^\mu_{TV}\cdot\triangle(\vec{j}_{TV})_\mu\Big]\end{aligned} \tag{5}$$

NO non-integer power of density terms!

Energy density functional

Pairing part

A density-independent δ-force in the pairing channel is adopted and the corresponding pairing energy is as follows,

$$\mathcal{E}^{\mathrm{pair}}[\kappa,\kappa^*] = \sum_{\tau=n,p} \mathrm{Tr}[\kappa_\tau^* \cdot V_\tau \cdot \kappa_\tau]. \tag{6}$$

Hohenberg-Kohn theorem and Kohn-Sham scheme

– According to the HK theorem, all the ground-state properties of interacting system are determined by the ground-state density $\rho_{\mathrm{gs}}^{\mathrm{I}}$, which minimizes the total energy. *P. Hohenberg and W. Kohn, Phys. Rev. 136 (1964) B864.*

– According to the KS scheme, there exist a unique local single-particle potential $\Sigma_{\mathrm{sp}}(\mathbf{r})$, such that the exact ground-state density $\rho_{\mathrm{gs}}^{\mathrm{I}}$ of interacting system equals the local ground-state density $\rho_{\mathrm{gs}}^{\mathrm{NI}}(\mathbf{r})$ of the auxiliary non-interacting system. *W. Kohn and L. J. Sham, Phys. Rev. 140, A1133 (1965)*

Relativistic analogue of Kohn-Sham equation

Auxiliary local densities/currents in the CDF theory

The local densities/currents in *no-sea* approximation are bilinear in the single-particle orbital ψ_k, weighted by the occupation probability v_k^2 or $u_k v_k$,

$$\Gamma_i^\mu(\mathbf{r}) = \sum_{k>0} v_k^2 \bar{\psi}_k(\mathbf{r}) \Gamma_i^\mu \psi_k(\mathbf{r}), \quad \kappa_\tau(\mathbf{r}) = -\sum_{k>0}^{\tau} f_k u_k v_k \psi_k^\dagger(\mathbf{r}) \psi_k(\mathbf{r}). \tag{7}$$

where $\Gamma_i^\mu = 1, \gamma^\mu$, and $\vec{\tau}\gamma^\mu$ for the S, T, and TV channels respectively. f_k is a smooth cutoff as introduced in Ref. *[Krieger (1990)]* to avoid divergence.

Relativistic analogue of Kohn-Sham equation

The single-particle orbital ψ_k is determined by the relativistic Kohn-Sham equation,

$$[\gamma_\mu(i\partial^\mu - \Sigma^\mu) - (m + \Sigma_S)]\,\psi_k = 0, \tag{8}$$

where the single-particle potentials (Σ_S,Σ^μ) are given in terms of densities,

$$\Sigma_S = \alpha_S \rho_S + \beta_S \rho_S^2 + \gamma_S \rho_S^3 + \delta_S \triangle \rho_S, \tag{9a}$$

$$\Sigma^\mu = \alpha_V j_V^\mu + \gamma_V (j_V^\mu)^3 + \delta_V \triangle j_V^\mu + e\frac{1-\tau_3}{2} A^\mu + \alpha_{TV} \vec{\tau} \cdot \vec{j}_{TV}^\mu + \delta_{TV} \vec{\tau} \cdot \triangle \vec{j}_{TV}^\mu. \tag{9b}$$

Parametrization procedure

Fitting method

Levenberg-Marquardt method

Obsevables in fitting

– Binding energies of 60 spherical nuclei from O to Pb isotopes
– Charge radii of 17 spherical nuclei from O to Pb isotopes
– Empirical neutron pairing gaps for ^{122}Sn, ^{124}Sn, and ^{200}Pb
– Empirical proton pairing gaps for ^{92}Mo, ^{136}Xe, and ^{144}Sm

Fitting strategy

– Starting from the PC-LA and PC-F1 sets, we minimize the square deviation between the experimental observable $O_i^{\rm exp}$ and the calculated value $O_i^{\rm cal}$

$$\chi^2(\mathbf{a}) = \sum_i^N \left[\frac{O_i^{\rm exp} - O_i^{\rm cal}(\mathbf{a})}{\omega_i}\right]^2 . \qquad (10)$$

– In order to balance the influence of different observables, the weight ω_i is introduced and taken as 1.00 for binding energies, 0.02 for charge radii and 0.05 for empirical pairing gaps respectively.

The PC-PK1 parameter set

Table: The point-coupling constants and pairing strengthes of PC-PK1 set. The corresponding QCD-scaled coupling constants c_{ln} are given in the last column as well.

Coupling Constant	Value	Dimension	c_{ln}
α_S	-3.96291×10^{-4}	MeV^{-2}	-1.695
β_S	8.6653×10^{-11}	MeV^{-5}	1.628
γ_S	-3.80724×10^{-17}	MeV^{-8}	-3.535
δ_S	-1.09108×10^{-10}	MeV^{-4}	-0.277
α_V	2.6904×10^{-4}	MeV^{-2}	1.151
γ_V	-3.64219×10^{-18}	MeV^{-8}	-0.338
δ_V	-4.32619×10^{-10}	MeV^{-4}	-1.097
α_{TV}	2.95018×10^{-5}	MeV^{-2}	0.505
δ_{TV}	-4.11112×10^{-10}	MeV^{-4}	-4.171
V_n	-349.5	$\mathrm{MeV\ fm}^3$	
V_p	-330	$\mathrm{MeV\ fm}^3$	

Table: Comparison with other parameter sets for the descriptions of binding energies of 60 selected spherical nuclei and charge radii of 17 selected spherical nuclei, where the root mean square (rms) deviation $\Delta = \sum_i^N \sqrt{(O_i^{\mathrm{exp}} - O_i^{\mathrm{cal}})^2/N}$.

	PC-PK1	DD-PC1	PC-F1	PC-LA	NL3*
Δ_{BE}	1.33	3.09	2.60	2.64	2.88
Δ_{Rc}	0.019	0.019	0.017	0.023	0.022

– **Much better description for the binding energies and the same good description for the charge radii of candidate nuclei.**

Nuclear matter properties at the saturation density

Table: The predicted saturation properties for nuclear matter by PC-PK1 in comparison with those by DD-PC1, PC-F1, PC-LA, NL3* and PK1, including the binding energy per nucleon E/A, nucleon Dirac mass M_D^* and Landau mass $M_L^* = \sqrt{p_F^2 + M_D^{*2}}$, incompressibility K_0, symmetry energy $E_{\rm sym}$, the slope $L \equiv 3\rho_0(dE_{\rm sym}/d\rho)_{\rho=\rho_0}$ and curvature $K_{\rm sym} \equiv 9\rho_0^2(d^2E_{\rm sym}/d^2\rho)_{\rho=\rho_0}$ of the symmetry energy at the saturation density ρ_0.

	PC-PK1	DD-PC1	PC-F1	PC-LA	NL3*	PK1
ρ_0 (fm^{-3})	0.154	0.152	0.151	0.148	0.150	0.148
$E/A(\mathrm{MeV})$	-16.12	-16.06	-16.17	-16.13	-16.31	-16.27
M_D^*/M	0.59	0.58	0.61	0.58	0.59	0.60
M_L^*/M	0.65	0.64	0.67	0.64	0.65	0.66
$K_0(\mathrm{MeV})$	238	230	255	264	258	283
$E_{\rm sym}(\mathrm{MeV})$	35.6	33	37.8	37.2	38.7	37.6
$L(\mathrm{MeV})$	113	70	117	108	123	116
$K_{\rm sym}(\mathrm{MeV})$	-583	-528	-627	-709	-630	-641

– **The saturation properties of nuclear matter (not adopted in fitting) are reproduced quite well.**

PW Zhao, ZP Li, JMY & J Meng, PRC82, 054319 (2010)

Binding energies of spherical nuclei

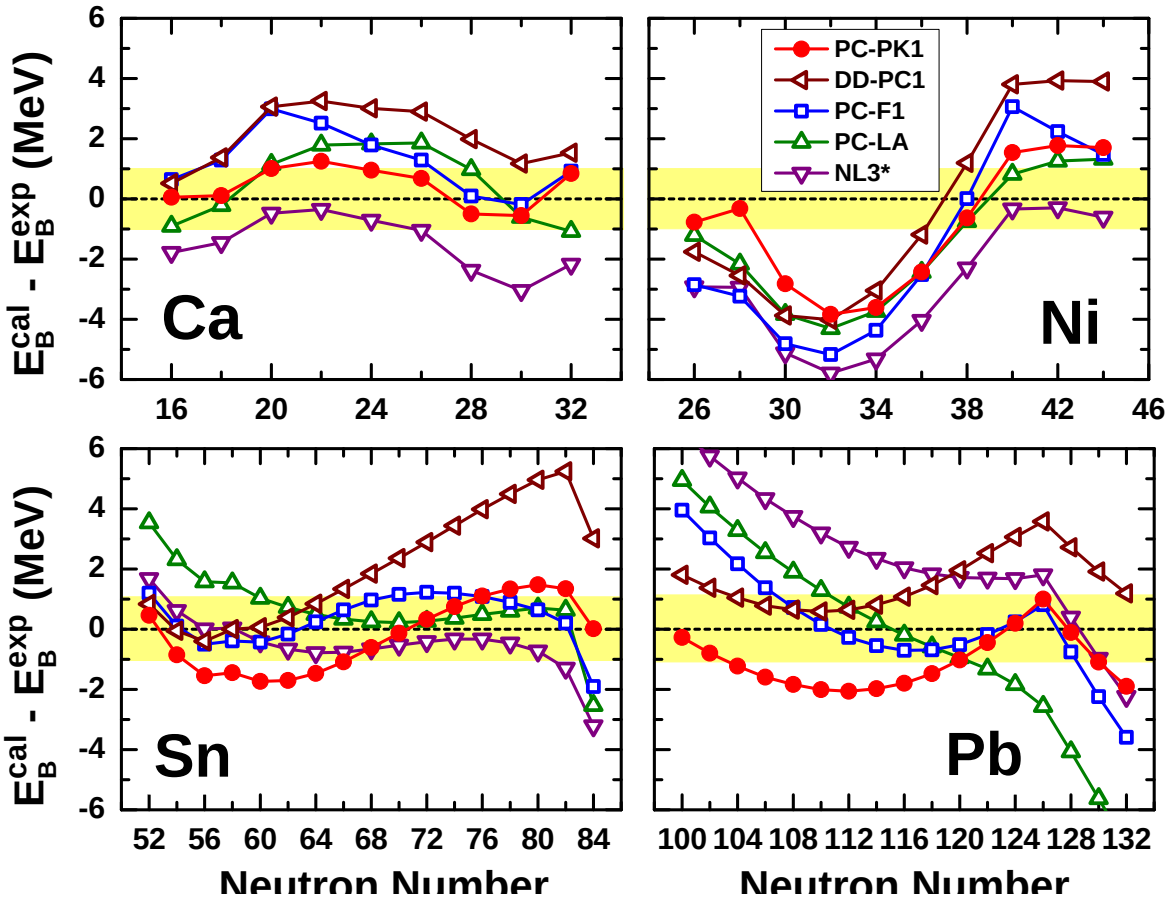

- The PC-PK1 well reproduces the binding energies.
- The small overall underestimation leaves space for dynamic correlation.

PW Zhao, ZP Li, JMY & J Meng, PRC82, 054319 (2010)

Binding energies of spherical nuclei

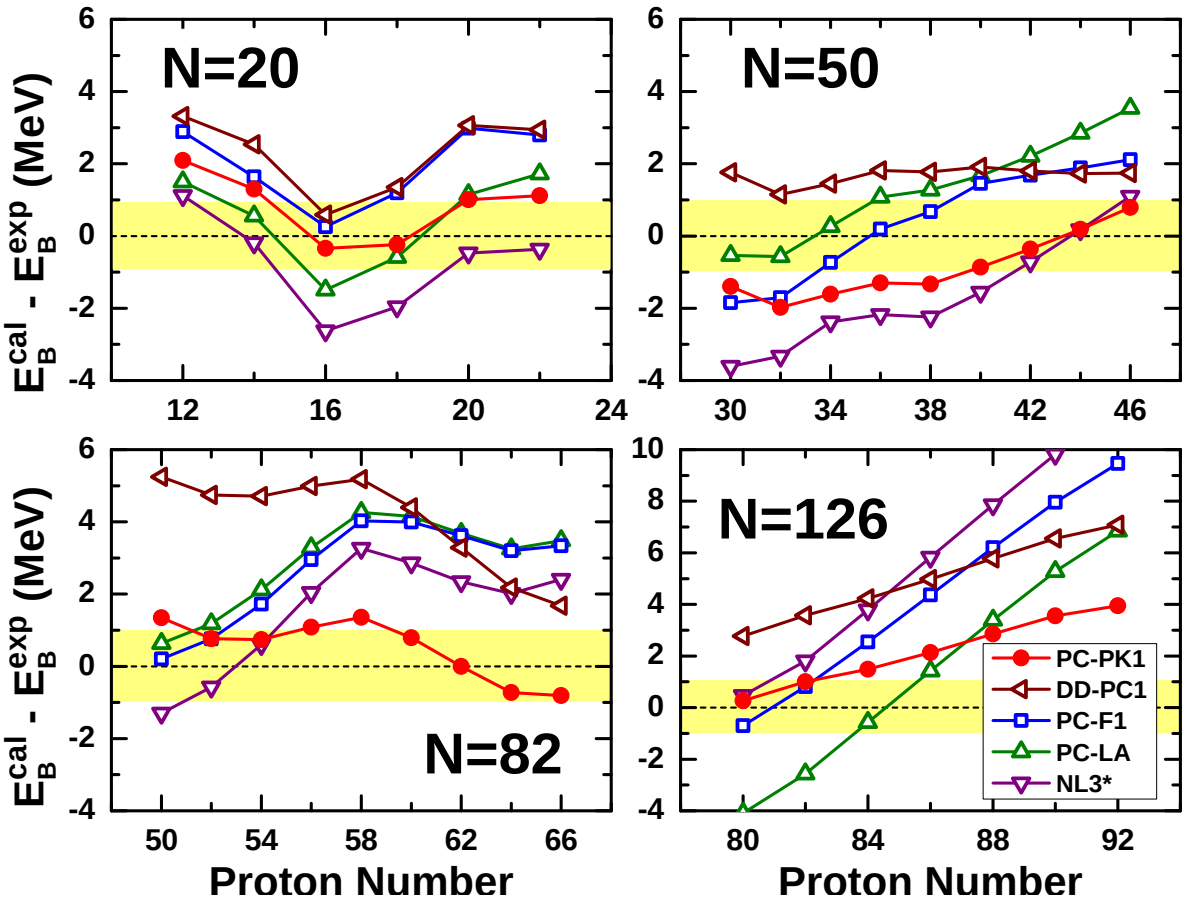

- A remarkable improvement is shown in the binding energies.
- The deviation is less isospin-dependent.

PW Zhao, ZP Li, JMY & J Meng, PRC82, 054319 (2010)

Binding energies of deformed nuclei: dynamic correlation energy

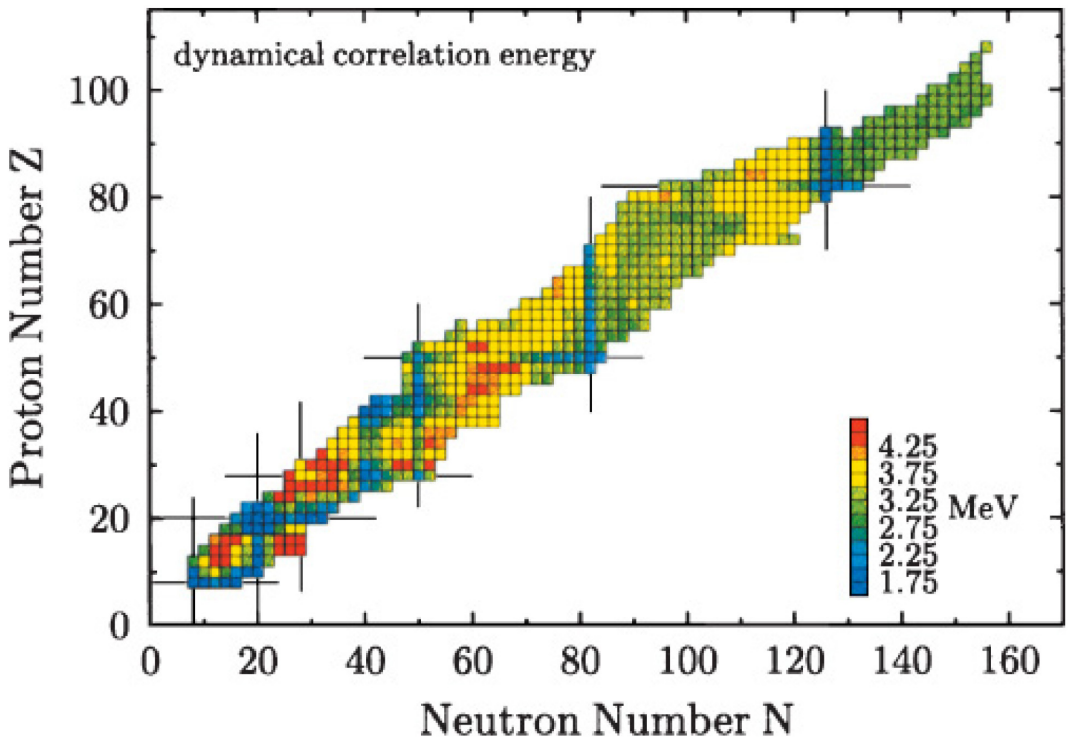

Global studies have shown that the dynamic (vibration and rotation) correlation energy in the ground state is

– the smallest for magic nuclei

– nearly constant (~ 3 MeV) for well deformed rare-earth and actinide nuclei

M. Bender, G. F. Bertsch & P.-H. Heenen, PRC73, 034322 (2006)

Binding energies of deformed nuclei: dynamic correlation energy

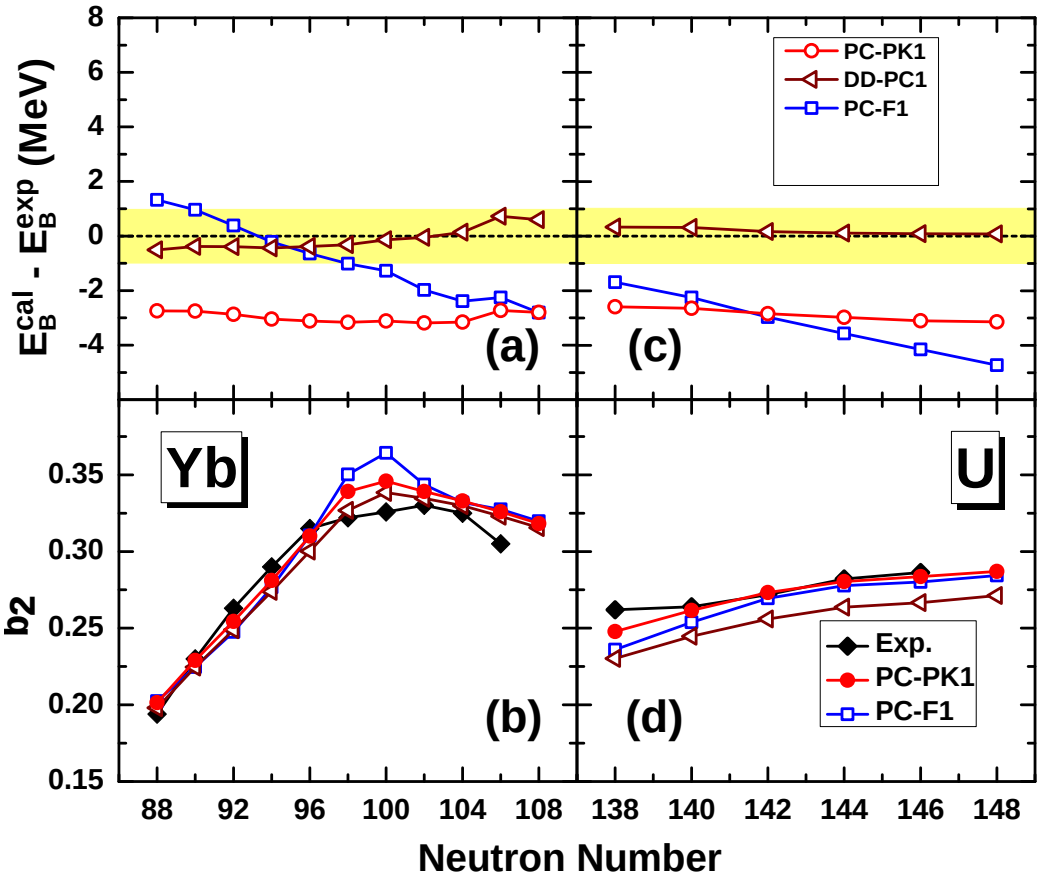

– **a systematic underestimation of the binding energies (~ 3 MeV)** for both ytterbium and uranium isotopes is found for PC-PK1.

PW Zhao, ZP Li, JMY & J Meng, PRC82, 054319 (2010)

Binding energies of deformed nuclei: dynamic correlation energy

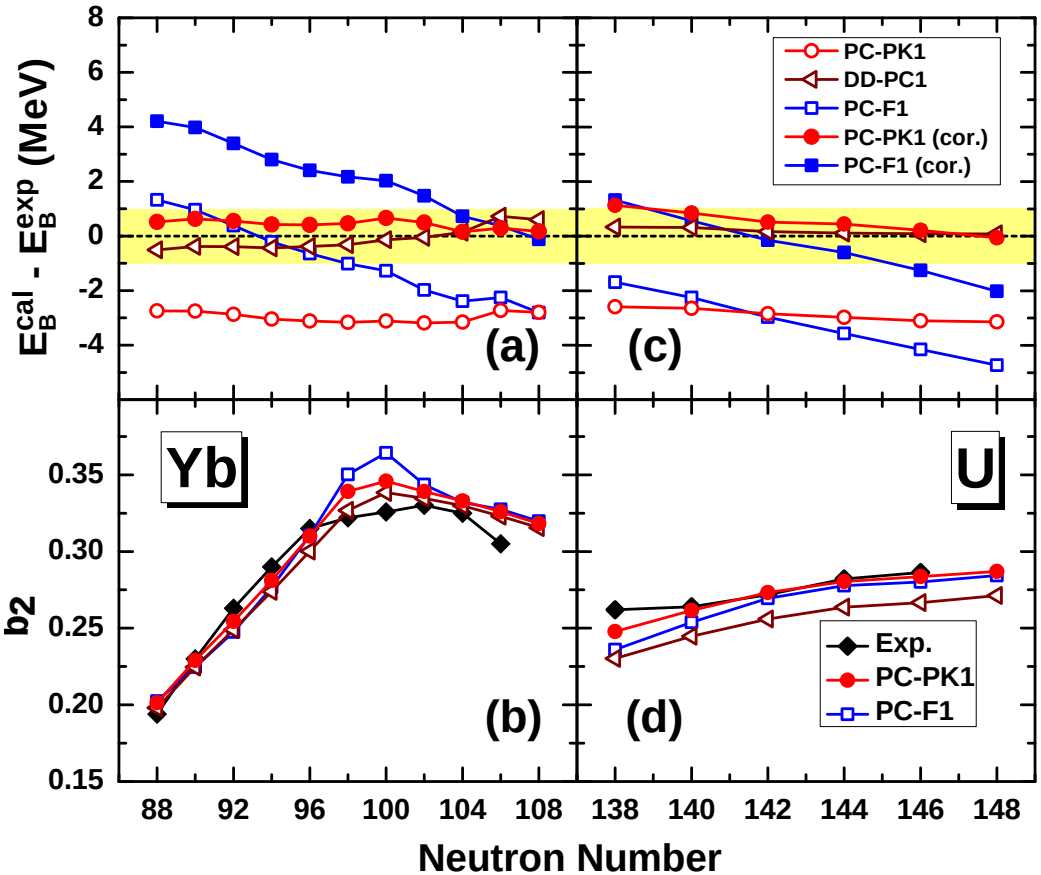

– After taking into account the rotational energy correction in the cranking approximation, **the deviations by PC-PK1 are within 1 MeV**.

PW Zhao, ZP Li, JMY & J Meng, PRC82, 054319 (2010)

Binding energies of deformed nuclei: dynamic correlation energy

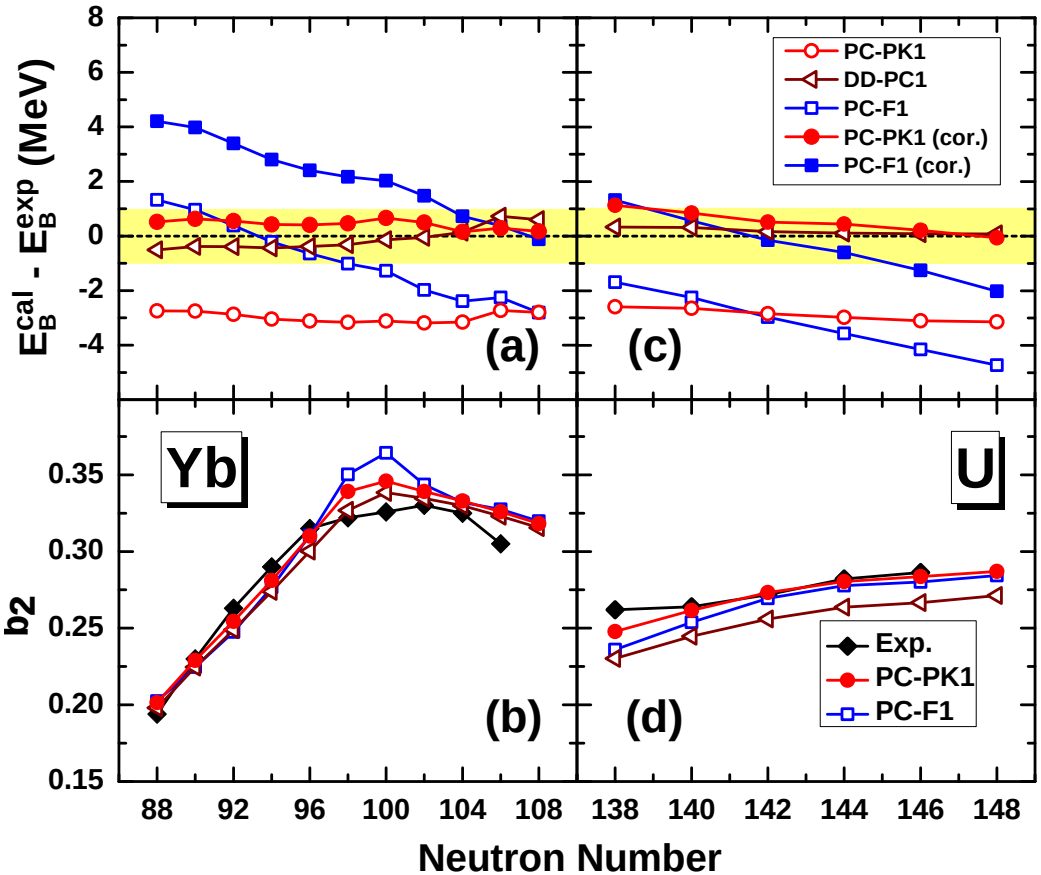

– The ytterbium and uranium isotopes were used to fit the **DD-PC1**, therefore there is no need to include additionally the rotational energy correction.

PW Zhao, ZP Li, JMY & J Meng, PRC82, 054319 (2010)

Outline

Configuration mixing of projected triaxial states

Construction of nuclear collective wave functions

The nuclear collective wave function of even-even nucleus is given by the superposition of projected triaxial states $|\Phi(\beta,\gamma)\rangle$ with designed quantum numbers J,

$$|\Psi^{JM}_{\alpha}\rangle = \int d\beta d\gamma \sum_{K\geq 0} f^{JK}_{\alpha} \mathcal{P}^{J}_{MK} |\Phi(\beta,\gamma)\rangle, \tag{11}$$

where $\mathcal{P}^{J}_{MK} = \frac{1}{(1+\delta_{K0})}[\hat{P}^{J}_{MK} + (-1)^{J}\hat{P}^{J}_{M-K}]$ is a symmetrized projection operator and $|\Phi(\beta,\gamma)\rangle$ is a set of quasi-particle vacua from the static covariant density functional calculations with constrains on the mass quadrupole moments.

Covariant energy functional with constrains on quadrupole moments

$$\mathcal{E}'[\rho_S, j^{\mu}_i, \kappa, \kappa^*] = \mathcal{E}_{\rm DF}[\rho_S, j^{\mu}_i, \kappa, \kappa^*] + \sum_{\mu=0,2} \frac{C_{\mu}}{2}(\langle \hat{Q}_{2\mu}\rangle - q_{2\mu})^2 \tag{12}$$

Note: A large set of highly correlated triaxially deformed states $|\Phi(\beta,\gamma)\rangle$ will be generated in the minimization of $\mathcal{E}'$ by changing the parameters $q_{2\mu}$.

Configuration mixing of projected triaxial states

Hill-Wheeler-Griffin (HWG) integral equation

The coefficients f_α^{JK} in the collective wave functions are determined by variation of the nuclear total energy $\mathcal{E}_\alpha^{JM}$ with respect to f_α^{JK*}.

$$\frac{\delta \mathcal{E}_\alpha^{JM}}{\delta f_\alpha^{JK}(q)} = \frac{\delta}{\delta f_\alpha^{JK*}} \left[\frac{\langle \Psi_\alpha^{JM} | \hat{H} | \Psi_\alpha^{JM} \rangle}{\langle \Psi_\alpha^{JM} | \Psi_\alpha^{JM} \rangle} \right] = 0. \tag{13}$$

This procedure is equivalent to the solution of following discretized Hill-Wheeler-Griffin (HWG) integral equation: $q \equiv (\beta, \gamma)$

$$\int dq' \sum_{K' \geq 0} \left[\mathscr{H}^J_{KK'}(q, q') - E^J_\alpha \mathscr{N}^J_{KK'}(q, q') \right] f_\alpha^{JK'}(q') = 0, \tag{14}$$

where $\mathscr{H}$ and $\mathscr{N}$ are the angular-momentum projected GCM kernel matrices of the Hamiltonian and the Norm, respectively.

Projected GCM kernel matrices

$$O^J_{KK'}(q, q') = \frac{2J+1}{8\pi^2} \int d\Omega D^{J*}_{KK'}(\Omega) \langle q | \hat{O} \hat{R}(\Omega) | q' \rangle \tag{15}$$

Multi-reference energy density functional

Transition/mixed density prescription for MR-EDF

In the projected Hamiltonian kernel, we adopt the transition/mixed density prescription [*Bonche, Dobaczewski, Flocard, Heenen & Meyer, NPA510, 466 (1990)*], i.e.,

$$\langle q|\hat{H}\hat{R}(\Omega)|q'\rangle/\langle q|\hat{R}(\Omega)|q'\rangle \longrightarrow \mathcal{E}^{MR}_{qq'}[\Gamma^{\mu}_{qq'}(\Omega)], \tag{16}$$

where the MR-EDF $\mathcal{E}^{MR}_{qq'}$ has the same form as the SR-EDF $\mathcal{E}^{SR}_{\rm DF}$, but replacing the densities/currents Γ^{μ} with the transition/mixed ones $\Gamma^{\mu}_{qq'}(\Omega)$, where $\Gamma^{\mu}_{qq}(0) = \Gamma^{\mu}$.

Local transition/mixed density/currents

$$\Gamma^{\mu}_{qq'}(\Omega)(\mathbf{r}) = \sum_{kl} \frac{\langle q|c^{\dagger}_k c_l \hat{R}(\Omega)|q'\rangle}{\langle q|\hat{R}(\Omega)|q'\rangle} \psi^{\dagger}_k(\mathbf{r})\Gamma^{\mu}\psi_l(\mathbf{r}) \tag{17}$$

Note: In the symmetry restored GCM calculations, the mixed density is in general a complex quantity and might be negative, and therefore can not be used in the EDFs with non-integer powers or exponential form of densities/currents.

Numerical implementation

Numerical details for mean-field calculations

- **Basis expansion method:** a set of three-dimensional isotropic harmonic oscillator basis functions in Cartesian coordinates
- **Symmetries**: parity, D_2 symmetry, and time reversal invariance

Numerical details for beyond-mean-field calculations

- A cutoff $\xi(=10^{-7})$ in the occupation probability to eliminate the contribution of high-lying s.p. states in the Dirac basis.
- The **Gaussian-Legendre quadrature** is used for integrals over the Euler angles in the calculations of kernels.
- **Symmetries in transition/mixed densities**: parity and time reversal invariance. The mixed (time-odd) currents are non-zero!
- **Symmetries in overlaps**: the symmetries imposed in the mean-field give rise to symmetries in the overlaps that allow the reduction of the integration intervals for the Euler angles by a factor of ~ 16.

JMY, J Meng, D Pena Arteaga & P Ring, Chin. Phys. Lett. 25, 3609 (2008);

JMY, J Meng, P Ring & D Pena Arteaga, PRC79, 044312 (2009);

JMY, J Meng, P Ring & D Vretenar, PRC81, 044311 (2010).

Numerical implementation

Solution of HWG equation

- Diagonalize the Norm matrix $\mathcal{N}^{J}_{KK'}(q,q')$ in both K and q spaces simultaneously and eliminate redundant degree of freedom.
- Construct a $\mathcal{H}$ matrix in *collective* subspace composed of *natural* states.
- Diagonalize the new $\mathcal{H}$ matrix in the *natural* basis and calculate the coefficients f^{JK}_{α} with the eigenvectors in the *collective* subspace.

P. Ring and P. Schuck, The Nuclear Many-Body Problem *(Springer, Heidelberg, 1980)*

Also introduced in the P.-H.Heenen's talk!

A approximate scheme correction for particle number projection

PN correction to MR-EDF

To account for the PNP correction, one usually subtracts two constraining terms from the MR-EDF,

$$\mathcal{E}^{MR}_{qq'}[\Gamma^{\mu}_{qq'}(\Omega)] \quad \rightarrow \quad \mathcal{E}^{MR}_{qq'}[\Gamma^{\mu}_{qq'}(\Omega)] - \lambda_p[Z_{q,q'}(\Omega) - Z_0] - \lambda_n[N_{q,q'}(\Omega) - N_0] \quad (18)$$

where Z/N_0 is the desired proton (neutron) number, $\lambda_\tau = (\lambda^q_\tau + \lambda^{q'}_\tau)/2$ and $Z/N_{q,q'}(\Omega) = \mathrm{Tr}[\Gamma^0_{qq'}(\Omega)(\mathbf{r})]$.

A approximate scheme correction for particle number projection

PN correction to MR-EDF

To account for the PNP correction, one usually subtracts two constraining terms from the MR-EDF,

$$\mathcal{E}^{MR}_{qq'}[\Gamma^{\mu}_{qq'}(\Omega)] \quad \rightarrow \quad \mathcal{E}^{MR}_{qq'}[\Gamma^{\mu}_{qq'}(\Omega)] - \lambda_p[Z_{q,q'}(\Omega) - Z_0] - \lambda_n[N_{q,q'}(\Omega) - N_0] \quad (18)$$

where Z/N_0 is the desired proton (neutron) number, $\lambda_\tau = (\lambda^q_\tau + \lambda^{q'}_\tau)/2$ and $Z/N_{q,q'}(\Omega) = \mathrm{Tr}[\Gamma^0_{qq'}(\Omega)(\mathbf{r})]$.

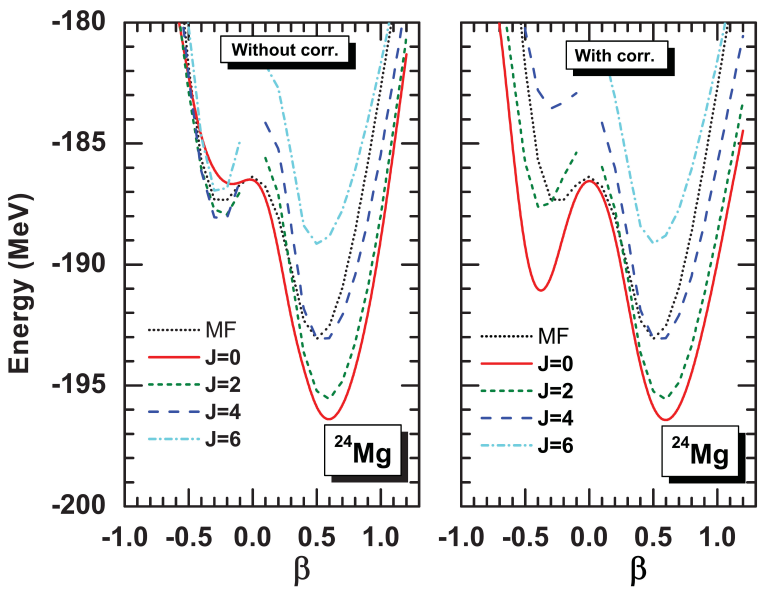

- Mean-field and projected energy curves of ^{24}Mg, calculated without (left panel) and with (right panel) the PN correction.
- Importance of the PN correction on the ordering of AMP PECs in certain regions of deformation.

JMY, H Mei, H Chen, J Meng, P Ring, & D Vretenar, PRC 83, 014308 (2011)

Convergence check of the angular momentum projection

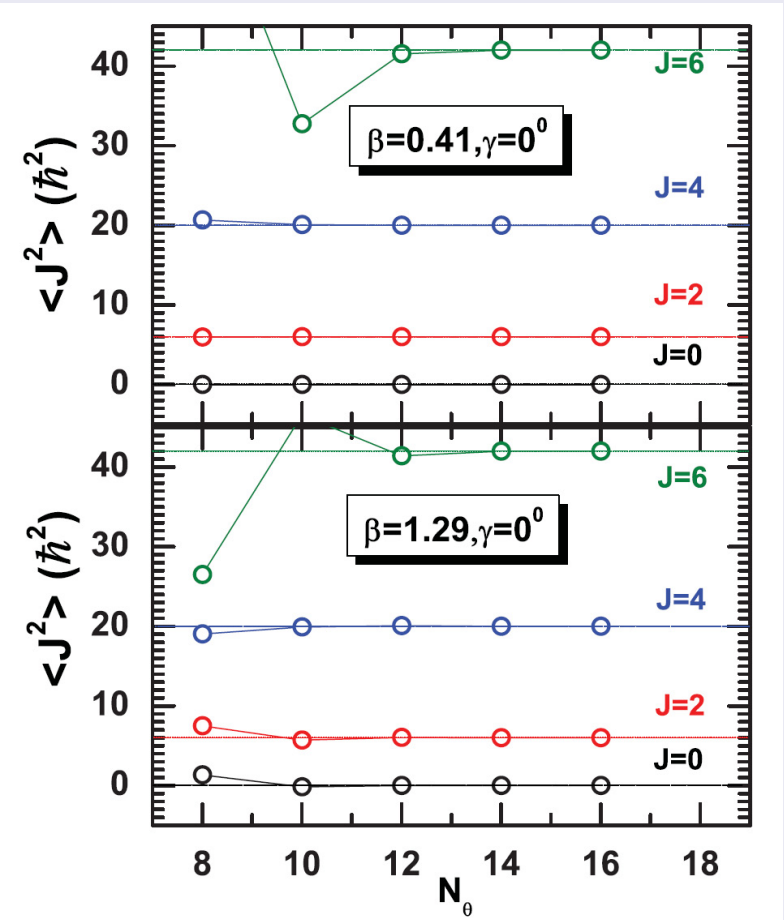

JMY, J Meng, P Ring, ZX Li, ZP Li & K Hagino, PRC 83, 014308 (2011)

- The expectation value of $\hat{J}^2$ on the projected state $|JMK;q\rangle$,

$$\begin{aligned} & \langle JMK;q|\hat{J}^2|JMK;q\rangle \\ = & \frac{\int d\Omega D^{J*}_{MK}\langle \hat{J}^2\hat{R}(\Omega)\rangle}{\int d\Omega D^{J*}_{MK}\langle \hat{R}(\Omega)\rangle} \\ = & J(J+1)\hbar^2, \end{aligned} \tag{19}$$

  where $\Omega = (\phi, \theta, \psi)$.
- $N_\theta = 10(12)$ is sufficient for the axial state with $J \leq 4(6)$.

Convergence check of the angular momentum projection

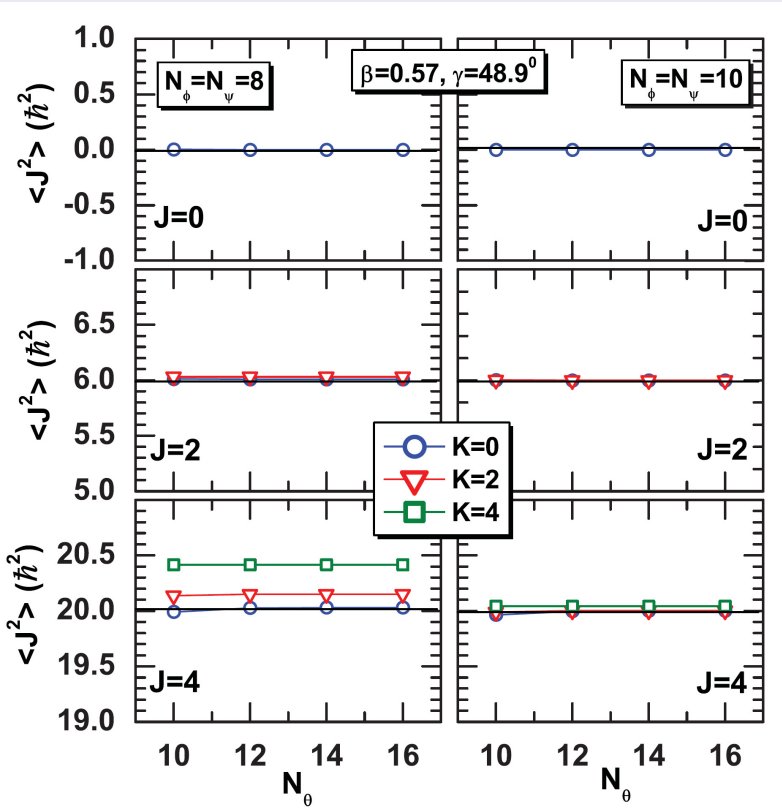

JMY, J Meng, P Ring, ZX Li, ZP Li & K Hagino, PRC 83, 014308 (2011)

- The expectation value of $\hat{J}^2$ on the projected state $|JMK;q\rangle$,

$$\begin{aligned} & \langle JMK;q|\hat{J}^2|JMK;q\rangle \\ = & \frac{\int d\Omega D^{J*}_{MK}\langle \hat{J}^2\hat{R}(\Omega)\rangle}{\int d\Omega D^{J*}_{MK}\langle \hat{R}(\Omega)\rangle} \\ = & J(J+1)\hbar^2, \end{aligned} \tag{19}$$

  where $\Omega = (\phi, \theta, \psi)$.
- $N_\theta = 10(12)$ is sufficient for the axial state with $J \leq 4(6)$.
- $N_{\phi,\psi} = 8(10)$ is sufficient for the triaxial state with $J \leq 2(4)$. The larger K component requires more mesh points for ϕ, ψ angles!
- $(N_\phi, N_\theta, N_\psi) = (10, 10, 10)$ is sufficient for the triaxial state with $J \leq 4$.

More mesh points in Euler angles for the states of higher spin states.

An example: the well deformed nucleus ^{166}Dysprosium

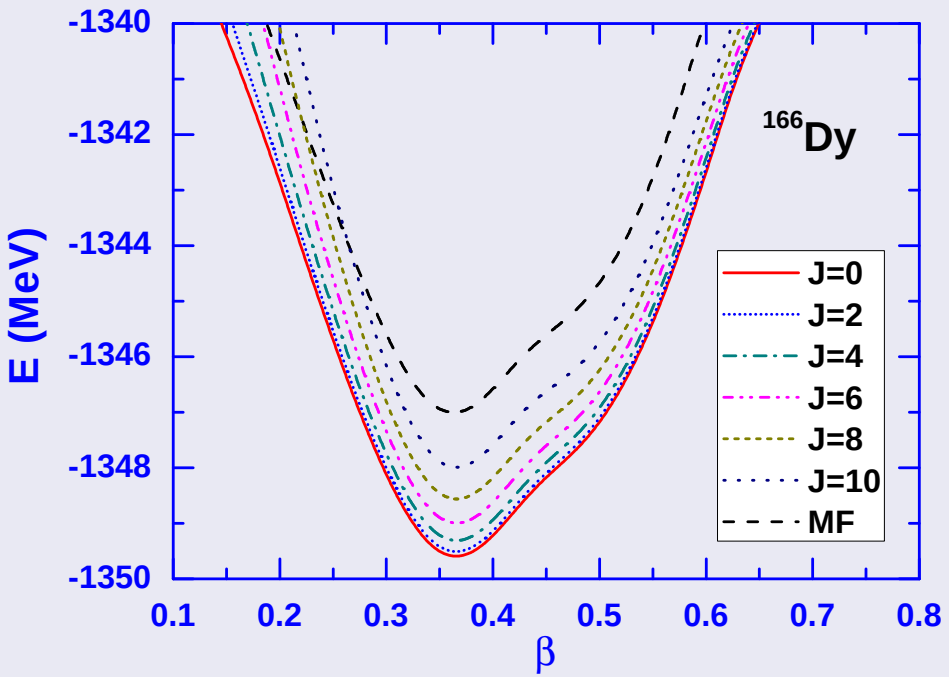

- A pronounced minimum with $\beta = 0.350$ in the mean-field potential energy surface.
- After angular momentum projection, one obtains the projected PES with $J = 0.\cdots, 10$.
- The projected PES with $J = 0$ has a minimum with $\beta = 0.375$.
- The energy gained from AMP is~ 3 MeV.

An example: the well deformed nucleus ^{166}Dysprosium

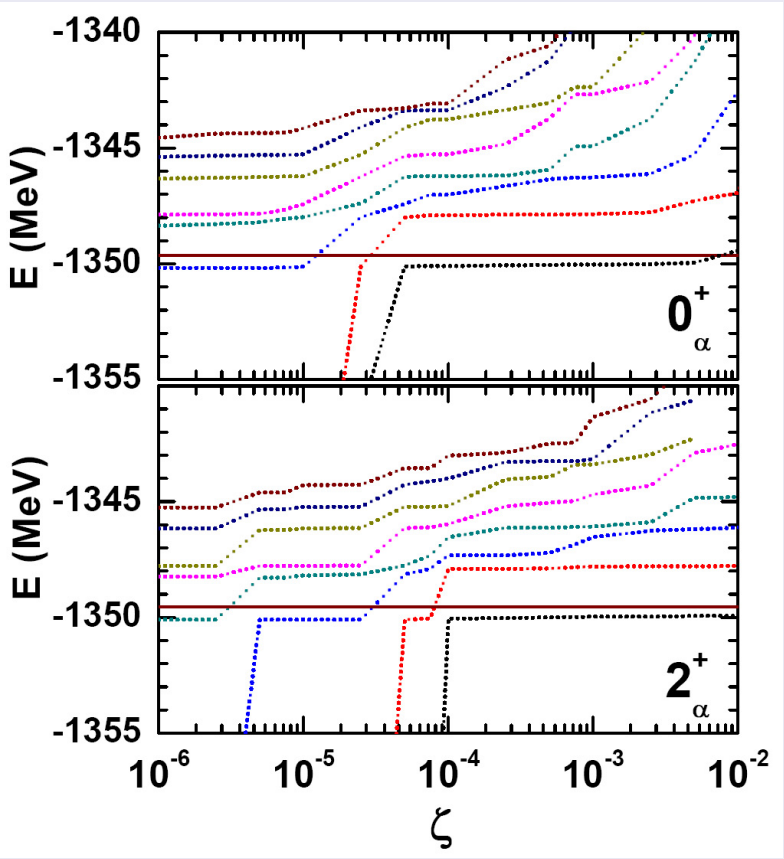

Figure: The energies of projected GCM states with $J = 0, 2$ as a function of the cutoff ζ used to define the *natural* basis. The horizontal line indicates the energy position for minimum on the projected PEC.

- The appearance of plateaus is the signature of the convergence of the GCM calculations. *P. Bonche, J. Dobaczewski, H. Flocard, P.-H. Heenen, and J. Meyer, Nucl. Phys. A 510, 466 (1990)*
- The ζ value should be the same for the same spin J state (orthogonality condition), but could be different for different spin states.

Also introduced in the Rodriguez's talk!

An example: the well axially deformed nucleus ^{166}Dysprosium

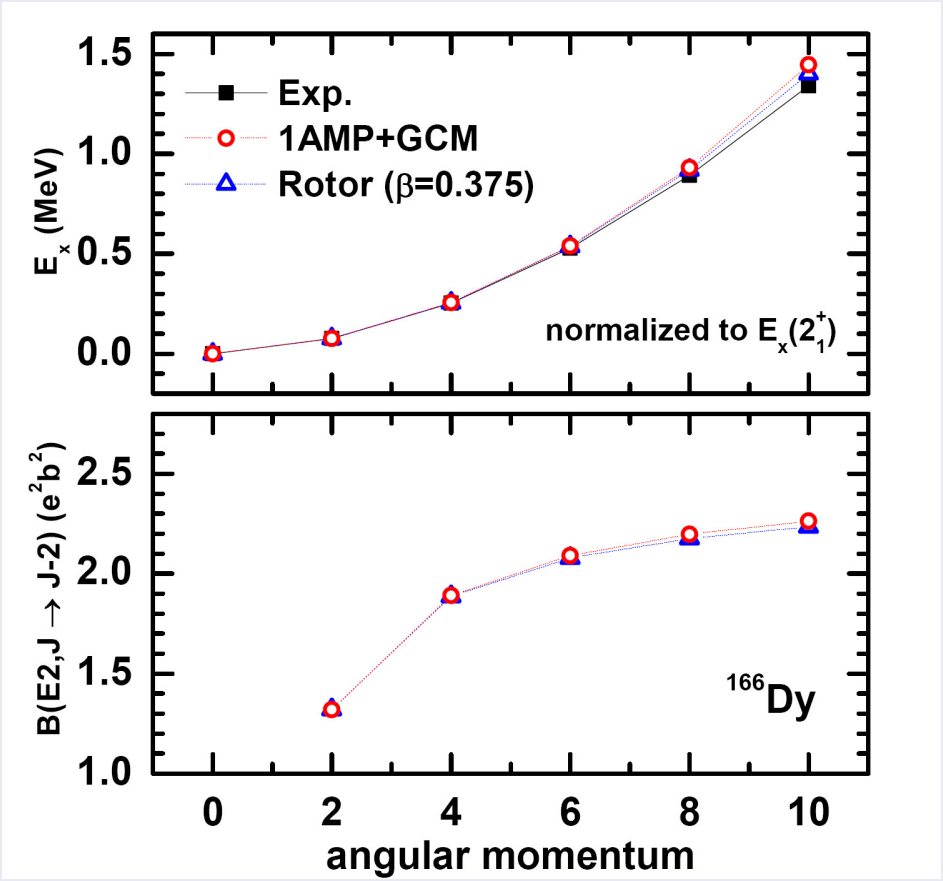

Figure: The excitation energies [normalized to $E_x(2_1^+)$] and $B(E2)$ values of low-lying states as functions of angular momentum.

- Good agreement has been shown between the rigid rotor model and the projected GCM calculations, both of which reproduce the data quite well.

1DAMP+GCM calculation for ^{80}Zr

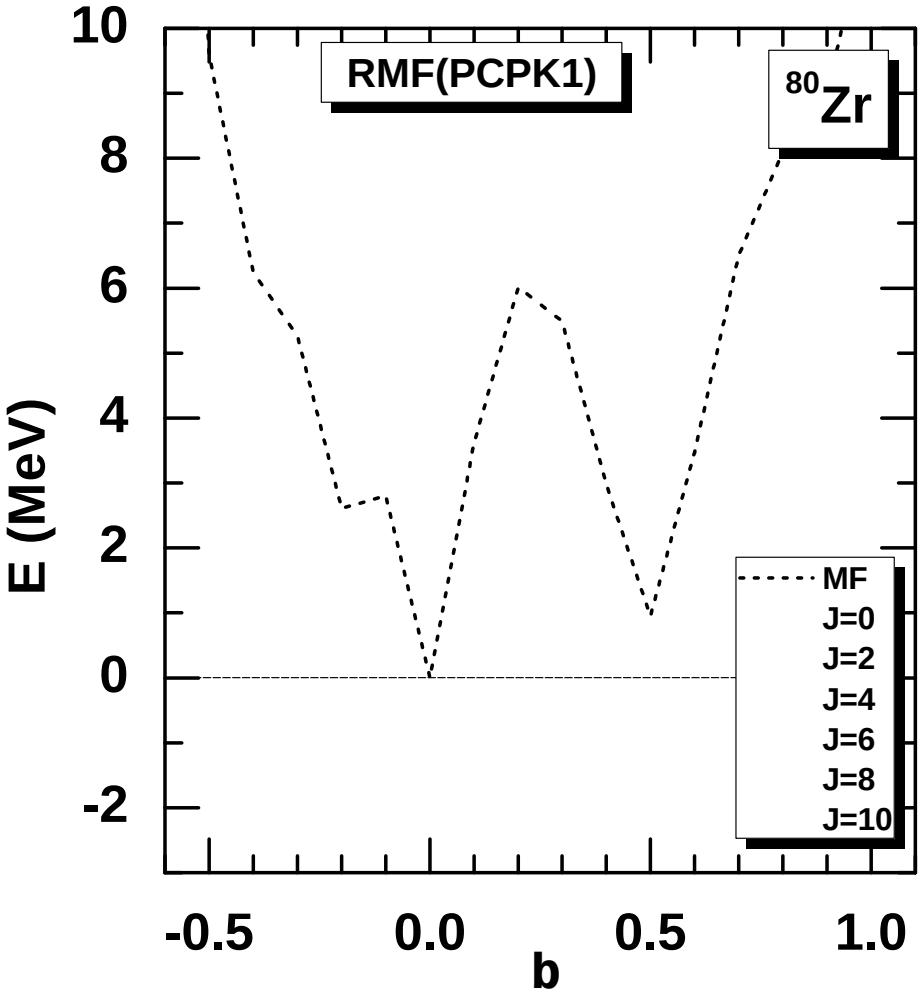

1DAMP+GCM calculation for ^{80}Zr

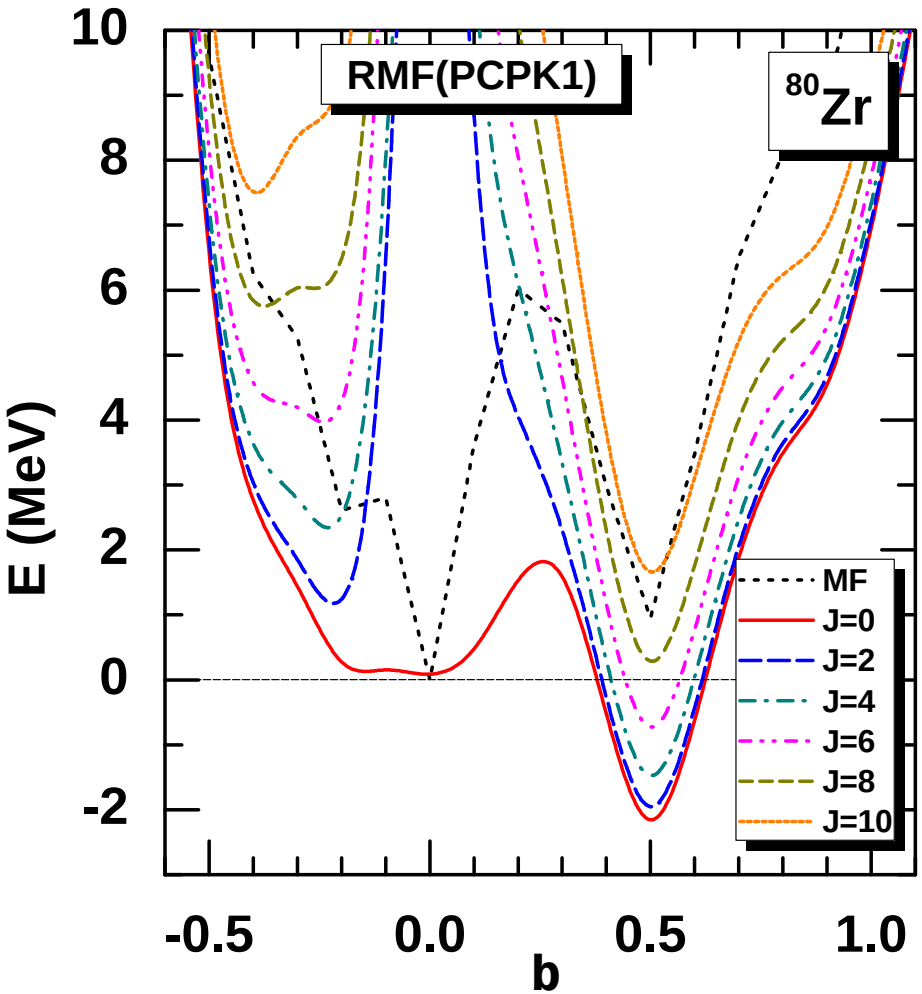

1DAMP+GCM calculation for ^{80}Zr

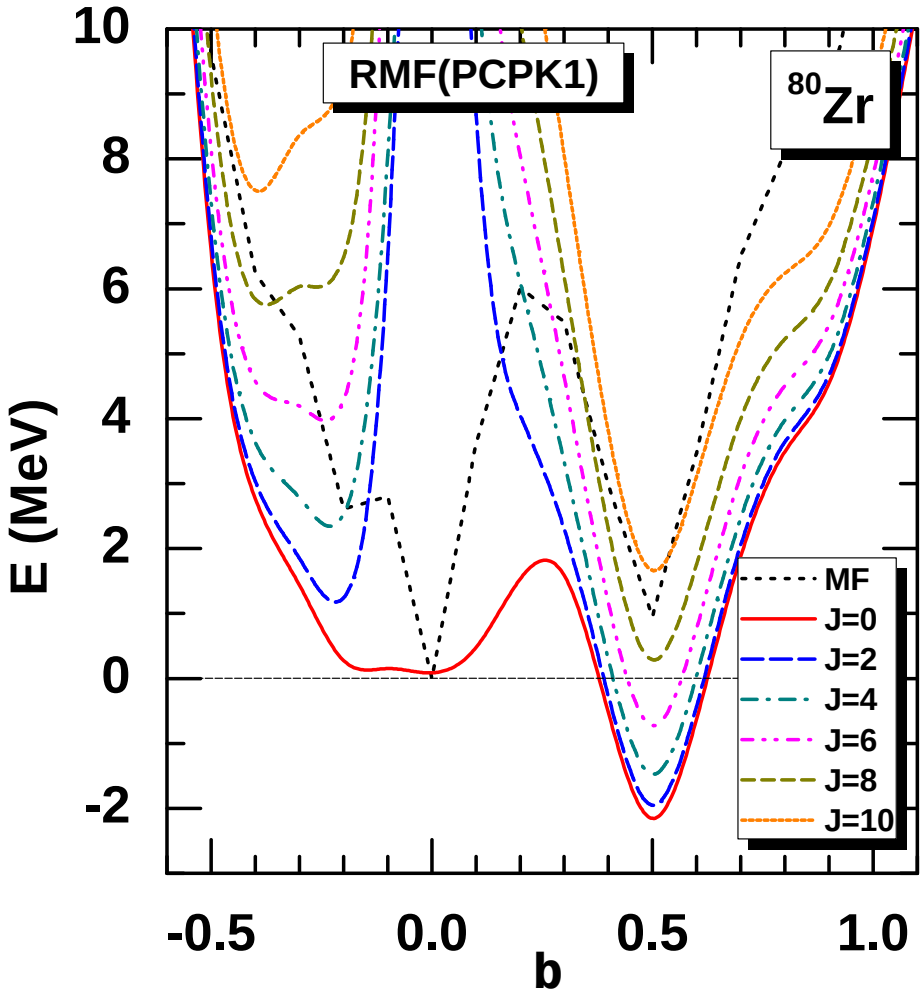

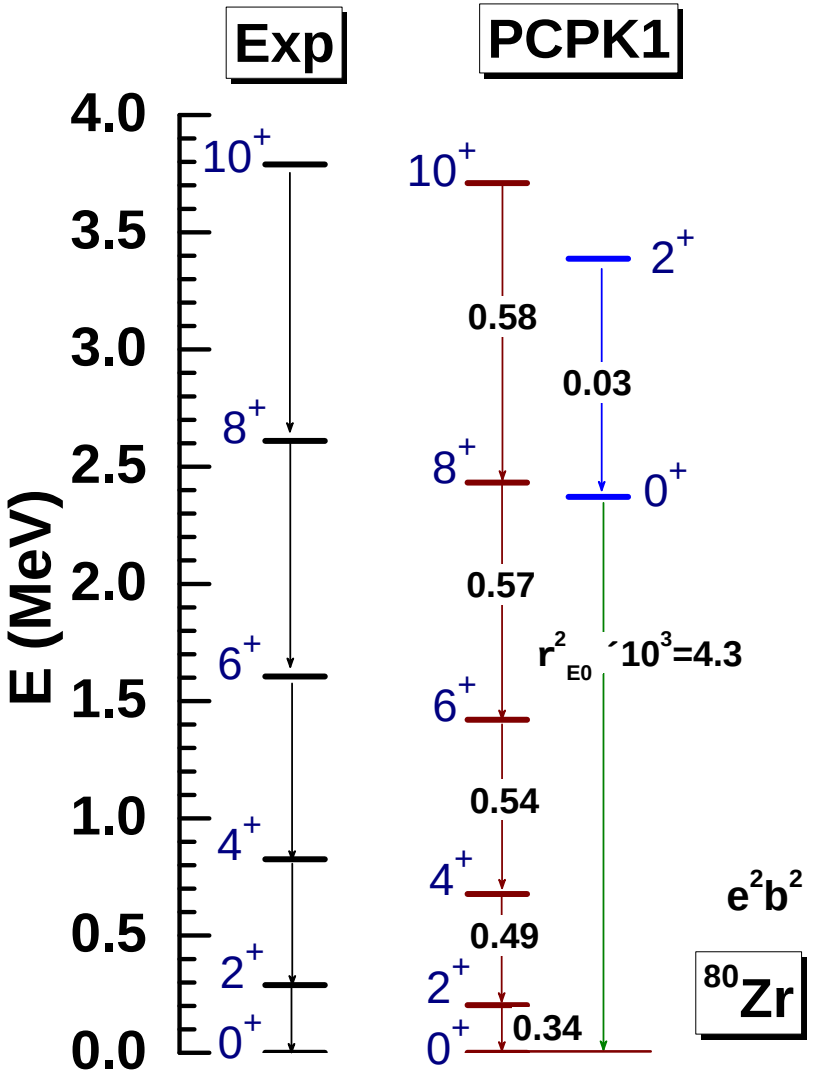

Example: ^{24}Mg

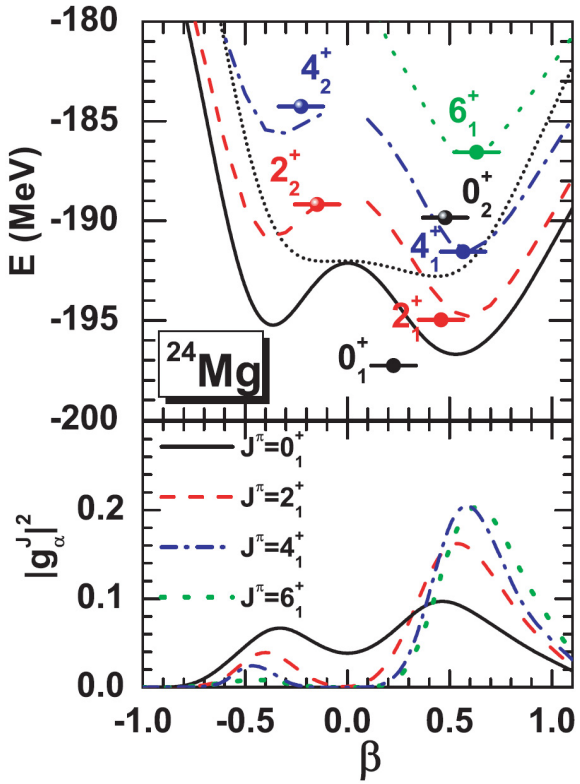

– **AMP generate two competing minima on the PEC($J = 0$).**

JMY, J Meng, P Ring,& D Vretenar, PRC81, 044311 (2010)

Example: ^{24}Mg

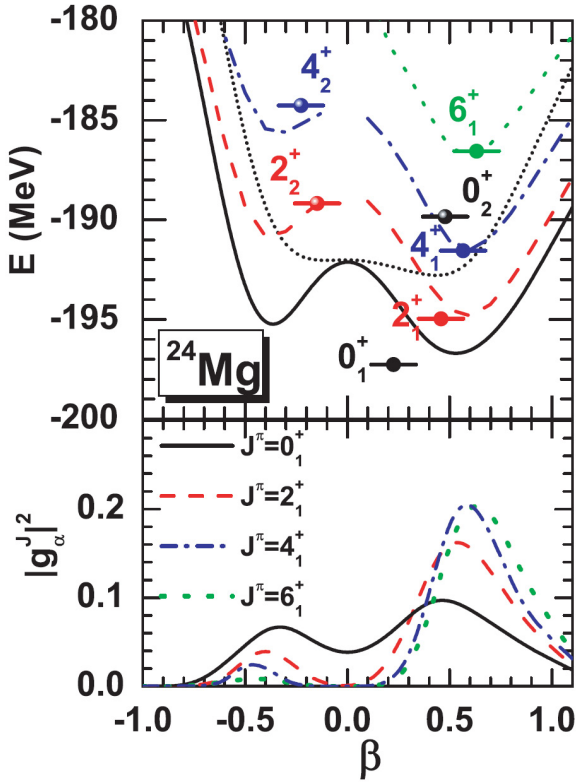

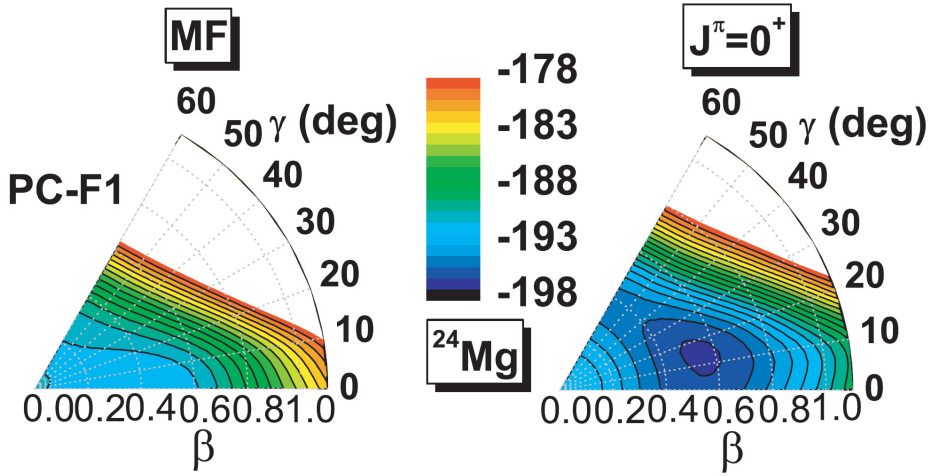

– **AMP generate two competing minima on the PEC($J = 0$).**

JMY, J Meng, P Ring,& D Vretenar, PRC81, 044311 (2010)

– **AMP deepens the energy of triaxial state (also shown in P. H. Heenen's talk!).**

Example: ^{24}Mg

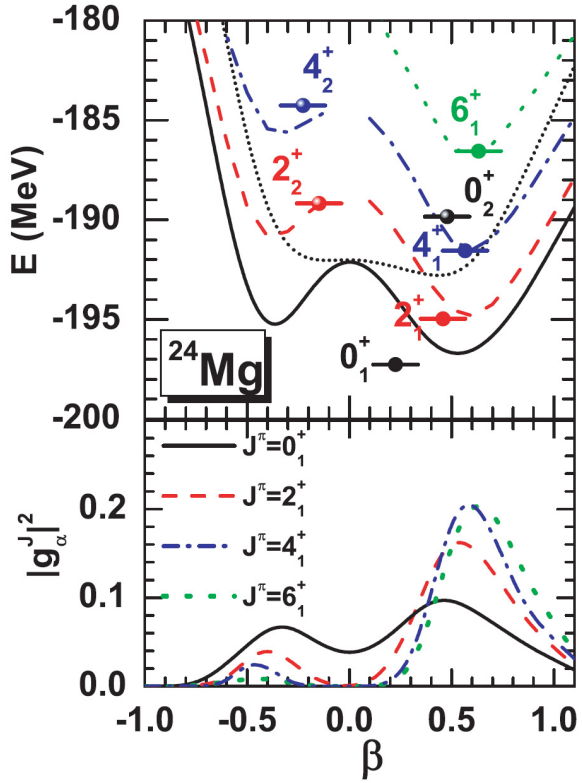

– AMP generate two competing minima on the PEC($J = 0$).

JMY, J Meng, P Ring,& D Vretenar, PRC81, 044311 (2010)

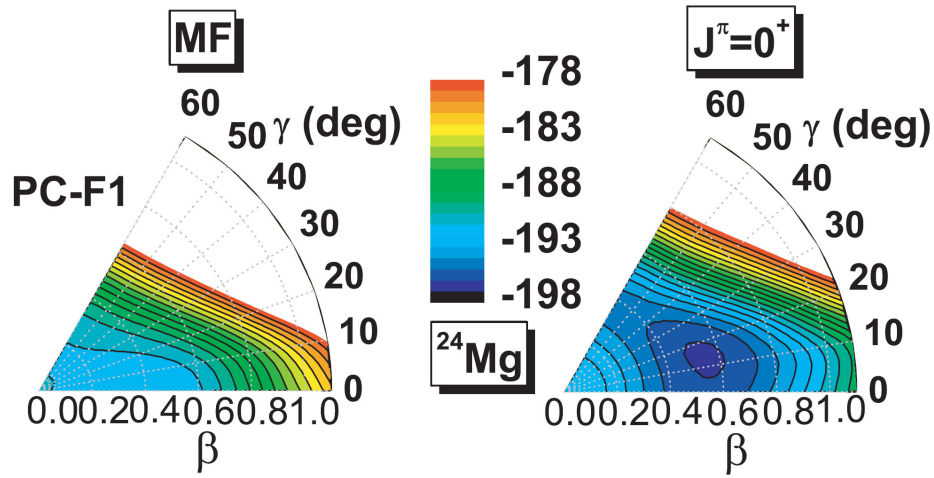

– AMP deepens the energy of triaxial state (also shown in P. H. Heenen's talk!).

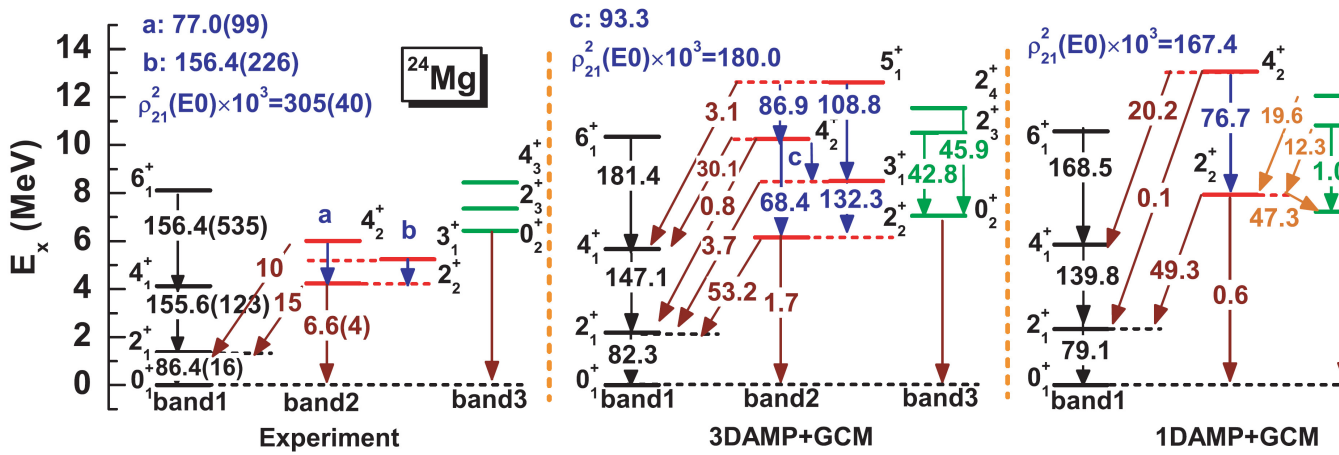

– The spectrum is reproduced rather well.

– Triaxiality increases slightly the collectivity of ^{24}Mg.

Potential energy curves of magnesium isotopes

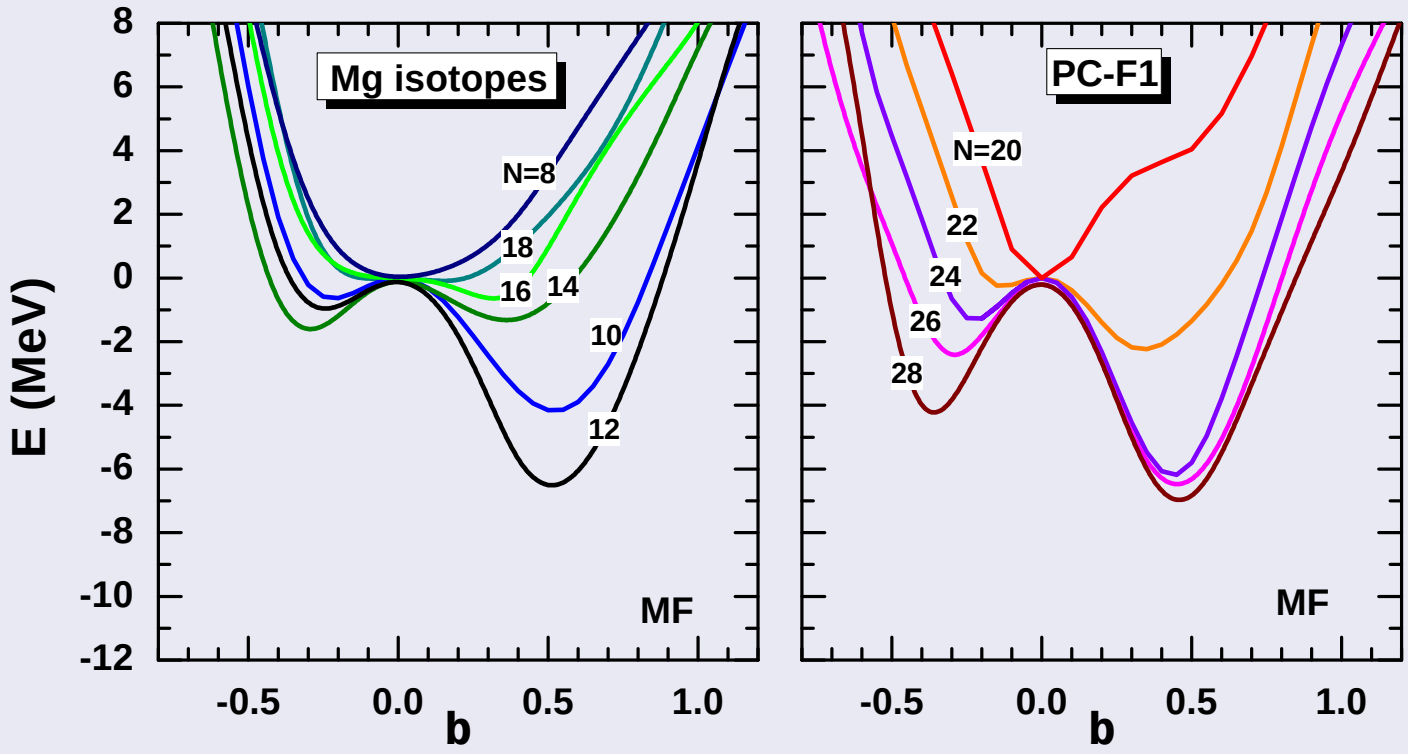

Figure: Self-consistent RMF+BCS mean-field potential energy curves of even-even magnesium isotopes, as functions of the axial deformation parameter β.

There are both prolate and oblate minima in most isotopes. The changing of global minima shows a clear picture of shape evolution with the neutron number: spherical (N=8) $\rightarrow$ deformed $\rightarrow$ spherical (N=20) $\rightarrow$ deformed

Potential energy curves of magnesium isotopes

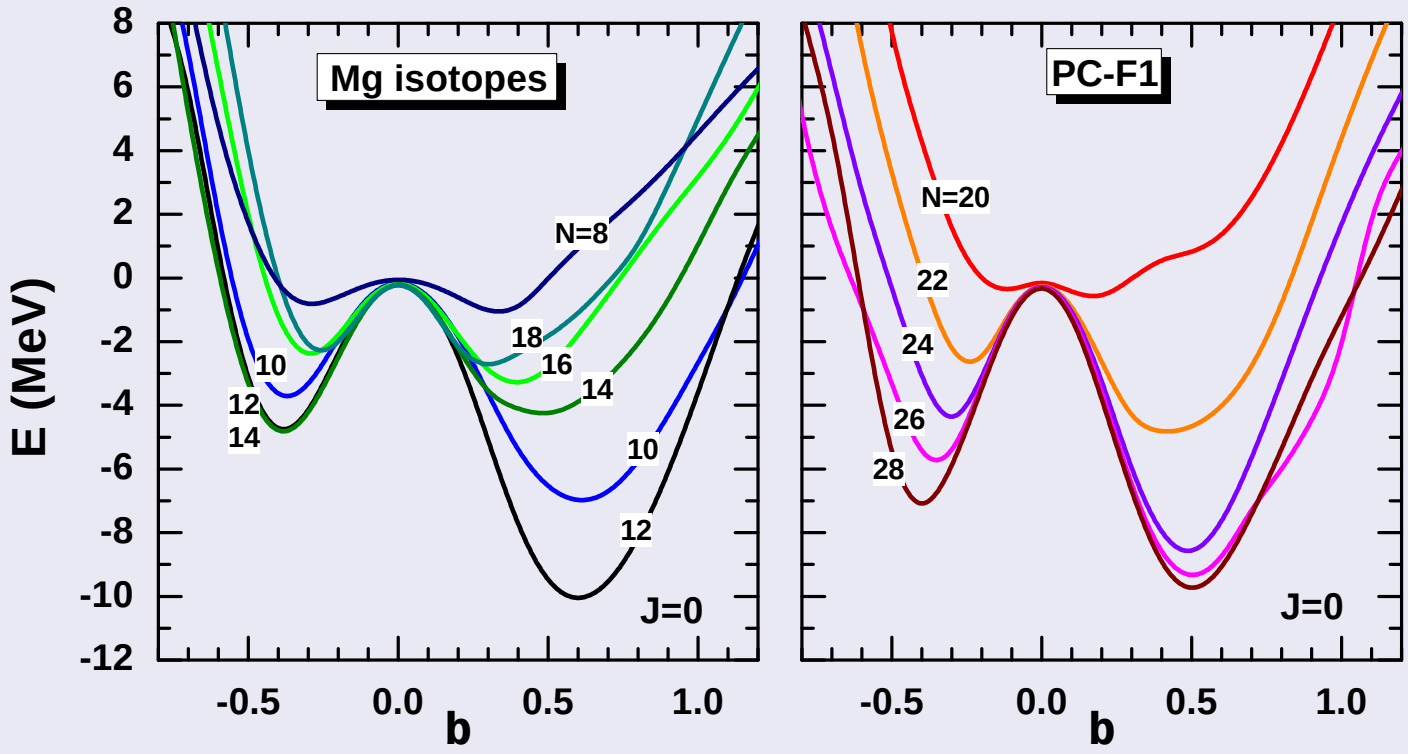

Figure: Angular-momentum projected 0^+ potential energy curves of even-even magnesium isotopes, as functions of the axial deformation parameter β.

The restoration of rotational symmetry lowers down the deformed minima and makes the spherical minima soft.

E2 transition strengths of magnesium isotopes

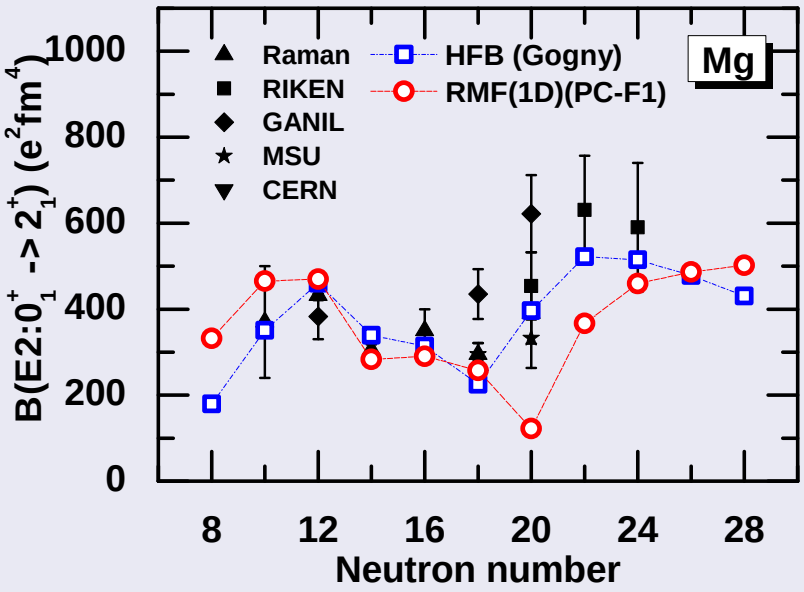

Figure: $B(E2; 0_1^+ \rightarrow 2_1^+)$ (e^2fm^4) values in $^{20-40}$Mg, calculated using the AMP+GCM model with the relativistic density functional PC-F1, are compared to available data and the results of the 1DAMP+GCM calculation based on the non-relativistic HFB framework with the Gogny force *[Rodriguez-Guzman, Egido & Robledo, NPA709, 201 (2002)]*.

- By restricting axial symmetry, the calculations with PC-F1 yield results in reasonable agreement with data except at and in the neighborhood of the neutron number $N = 20$.
- The PC-F1(PC-PK1) gives spherical g.s. for ^{32}Mg, contradicting with the data?

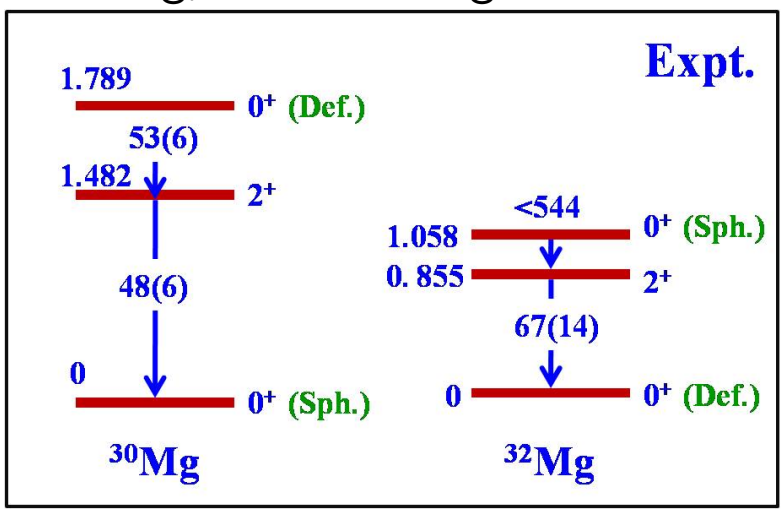

W. Schwerdtfeger et al., PRL 103, 012501 (2009); K. Wimmer et al., PRL 105, 252501 (2010)

The puzzle of ^{32}Mg! *Fortune, PRC84, 024327 (2011)*

- Triaxality or pairing correlation?

E2 transition strengths of magnesium isotopes

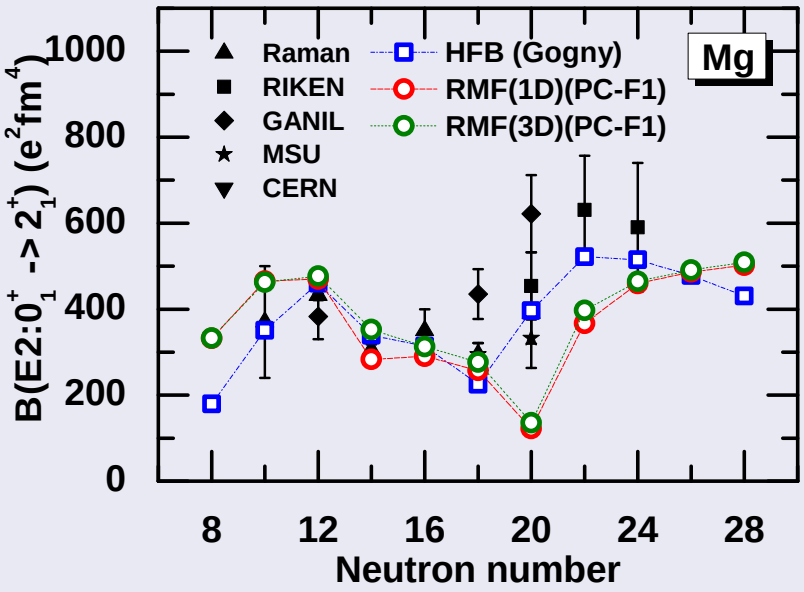

Figure: $B(E2; 0_1^+ \rightarrow 2_1^+)$ (e^2fm^4) values in $^{20-40}$Mg, calculated using the AMP+GCM model with the relativistic density functional PC-F1, are compared to available data and the results of the 1DAMP+GCM calculation based on the non-relativistic HFB framework with the Gogny force *[Rodriguez-Guzman, Egido & Robledo, NPA709, 201 (2002)]*.

- By restricting axial symmetry, the calculations with PC-F1 yield results in reasonable agreement with data except at and in the neighborhood of the neutron number $N = 20$.
- The PC-F1(PC-PK1) gives spherical g.s. for ^{32}Mg, contradicting with the data?

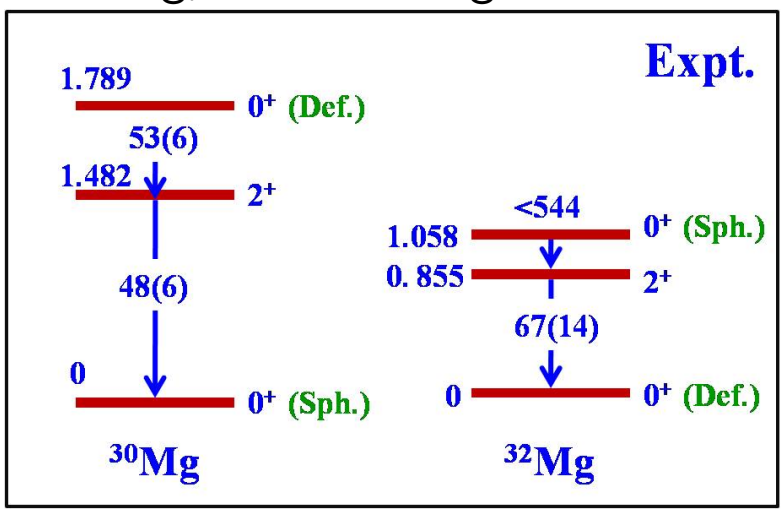

W. Schwerdtfeger et al., PRL 103, 012501 (2009); K. Wimmer et al., PRL 105, 252501 (2010)

The puzzle of ^{32}Mg! *Fortune, PRC84, 024327 (2011)*

- Triaxality or pairing correlation?

Different pairing strengths: δ force

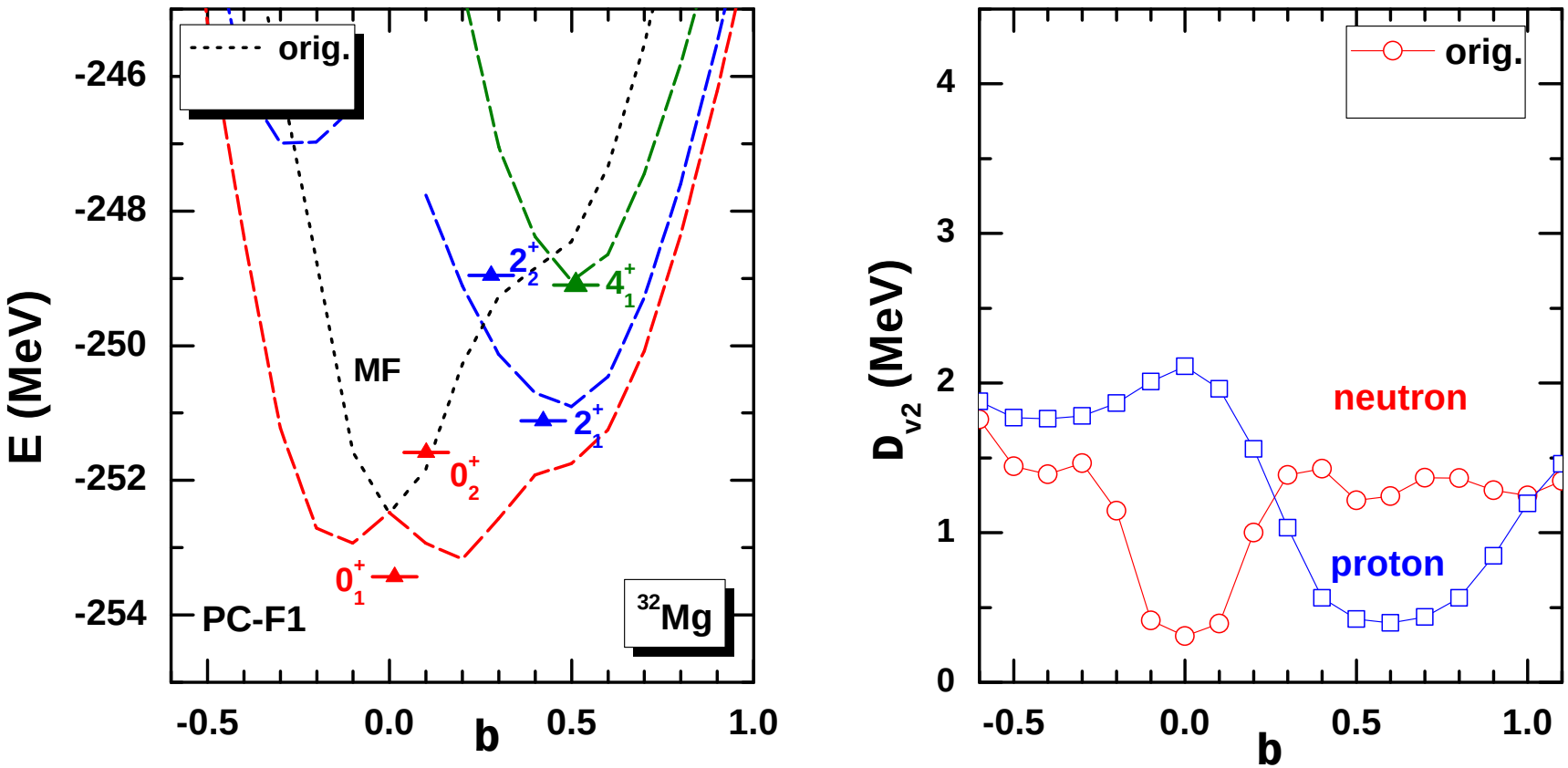

Orig.(δ^*): T. Burvenich, D. G. Madland, J. A. Maruhn, and P. G. Reinhard, PRC65, 044308 (2002)

Adju.(δ): JMY, J. Meng, P. Ring & D. P. Arteaga, PRC79, 044312 (2009)

Different pairing strengths: δ force

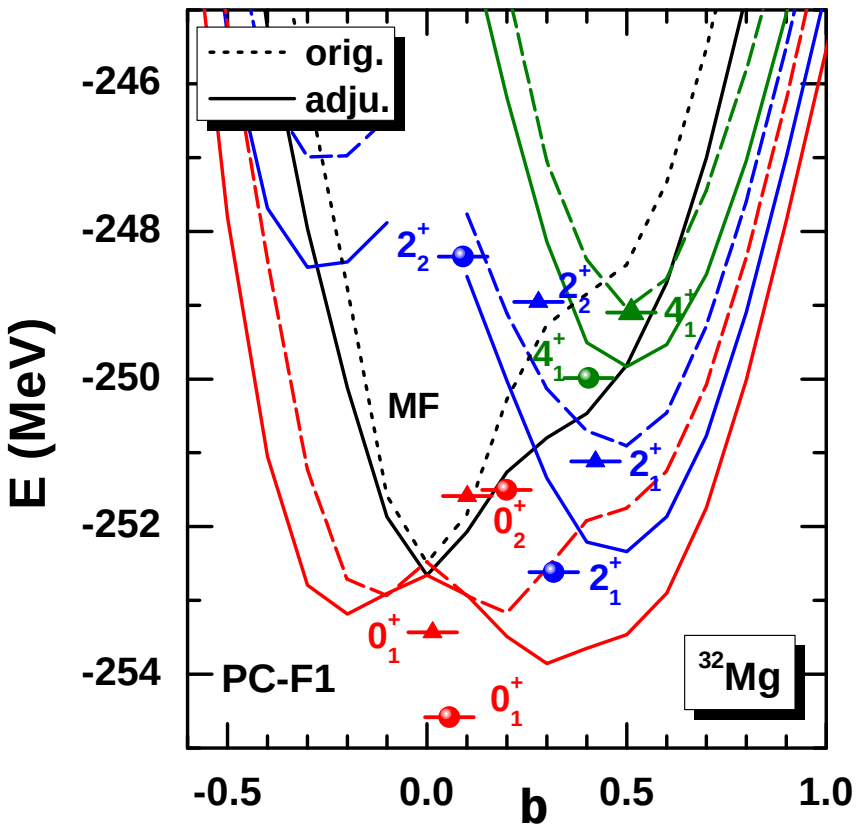

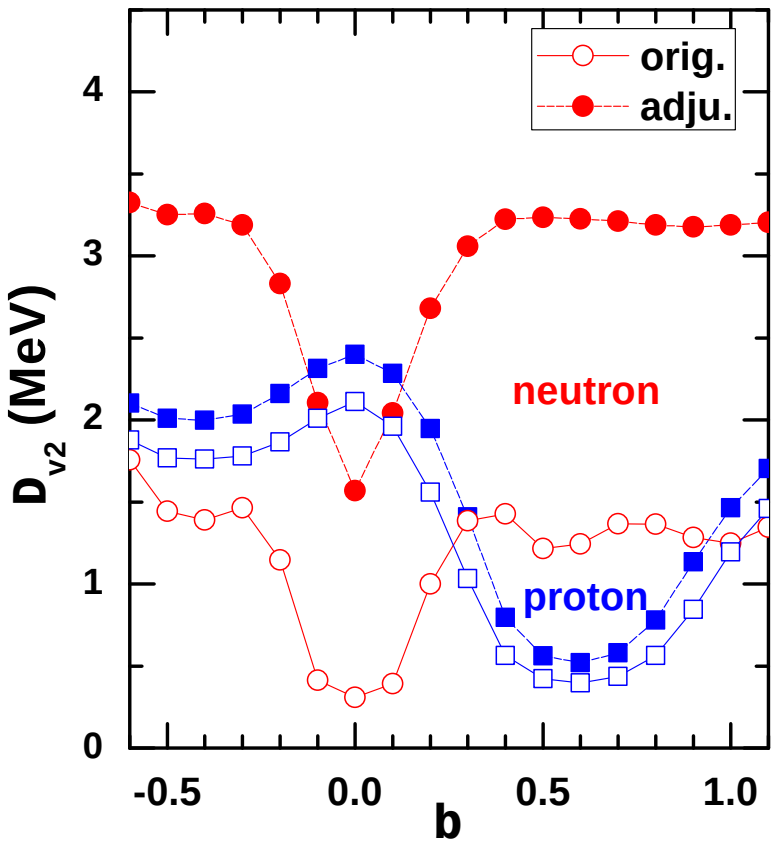

Orig.(δ^*): T. Burvenich, D. G. Madland, J. A. Maruhn, and P. G. Reinhard, PRC65, 044308 (2002)

Adju.(δ): JMY, J. Meng, P. Ring & D. P. Arteaga, PRC79, 044312 (2009)

Strengths of δ pairing force in ^{32}Mg

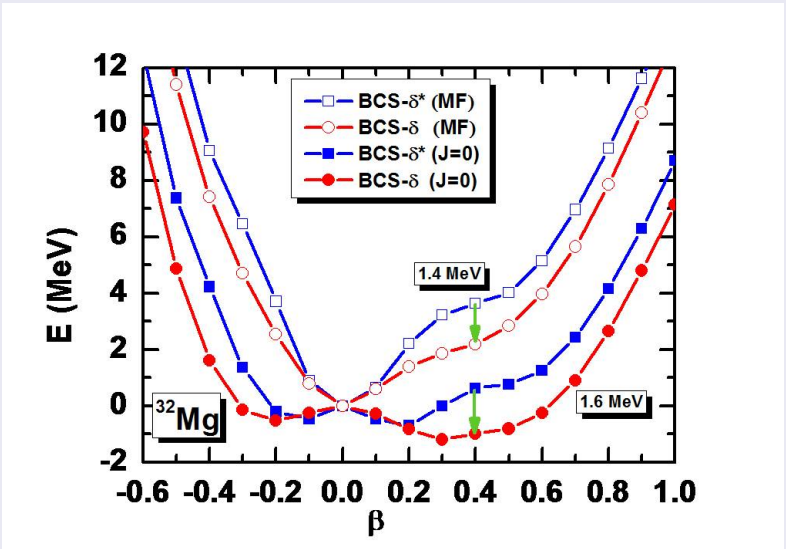

Adjusted pairing strengths (fitted to odd-even mass diff.) lower down the shoulder by 1.6 MeV. As a results, a prolate deformed minimum is shown on the projected ($J = 0$) PEC.

Strengths of δ pairing force in ^{32}Mg

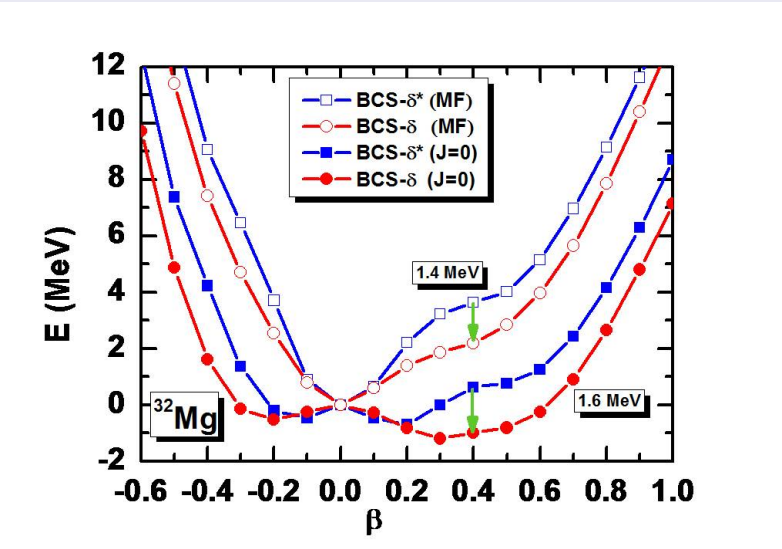

Adjusted pairing strengths (fitted to odd-even mass diff.) lower down the shoulder by 1.6 MeV. As a results, a prolate deformed minimum is shown on the projected ($J = 0$) PEC.

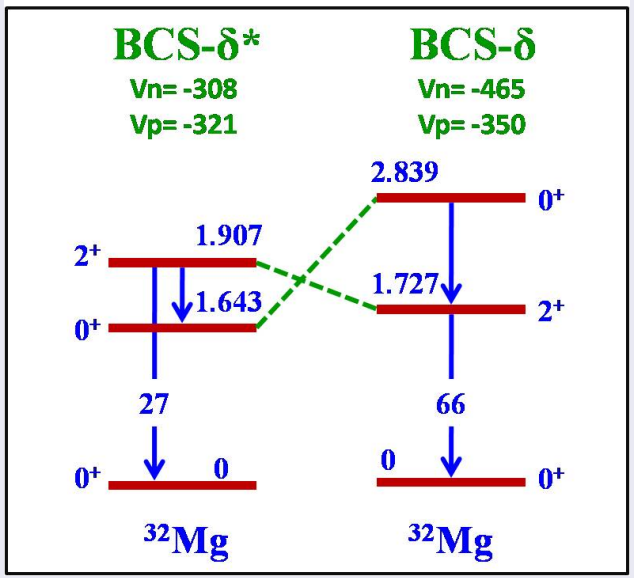

Results of the 3DAMPGCM calculations. The $B(E2; 0_1^+ \rightarrow 2_1^+) = 330.1$ e^{2}fm^4 and the ordering of 2_1^+ and 0_2^+ states in ^{32}Mg by the adjusted pairing strengths are in good agreement with the data.

Strengths of δ pairing force in ^{32}Mg

Distributions of wave functions:

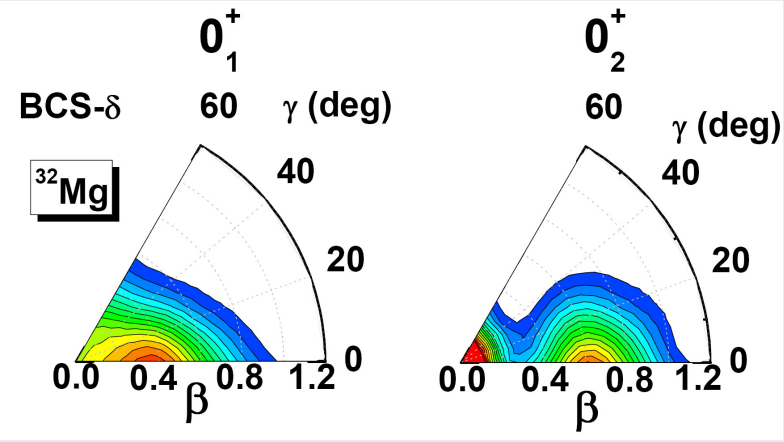

0_1^+: Prolate 0_2^+: Spherical and Prolate

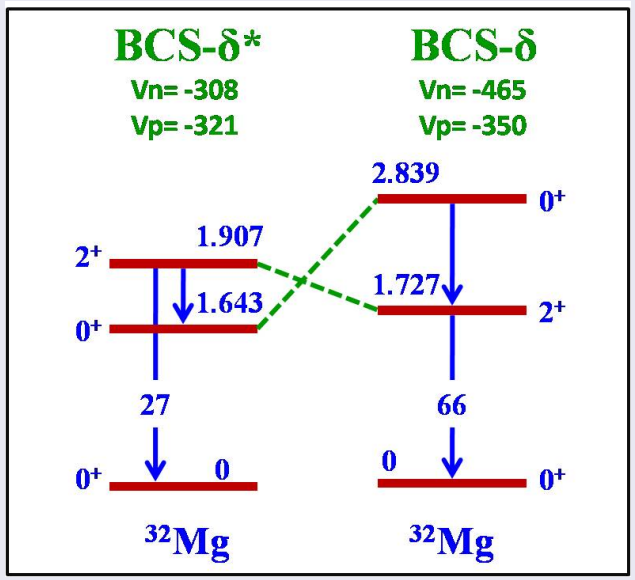

Results of the 3DAMPGCM calculations. The $B(E2; 0_1^+ \rightarrow 2_1^+) = 330.1$ e^{2}fm^4 and the ordering of 2_1^+ and 0_2^+ states in ^{32}Mg by the adjusted pairing strengths are in good agreement with the data.

Strengths of δ pairing force in ^{32}Mg

The strong pairing strength melts the $N = 20$ shell gap, as a consequence of which, the deformed configuration becomes the ground state.

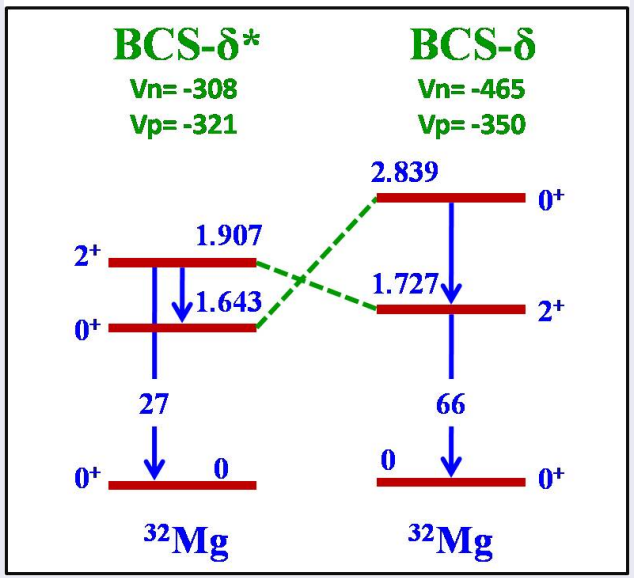

Results of the 3DAMPGCM calculations. The $B(E2; 0_1^+ \rightarrow 2_1^+) = 330.1$ e^{2}fm^4 and the ordering of 2_1^+ and 0_2^+ states in ^{32}Mg by the adjusted pairing strengths are in good agreement with the data.

Carbon isotopes

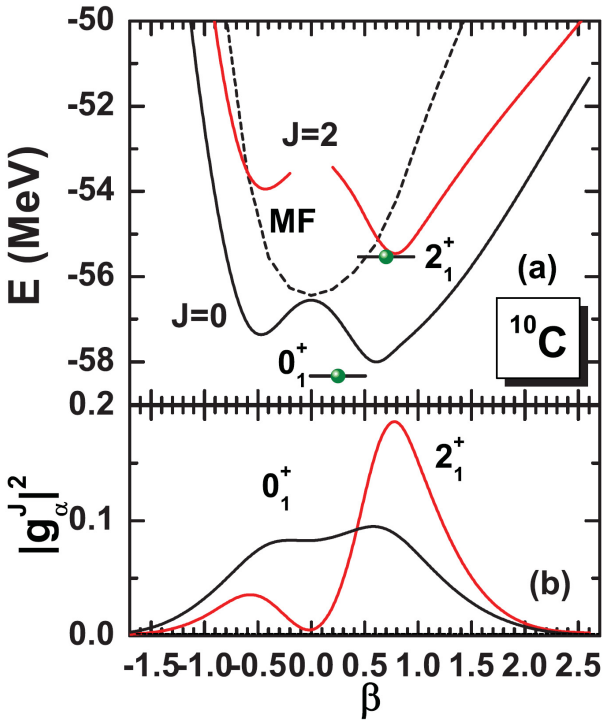

– Rather good agreement between the two calculations and the experiment data is found for the systematics of both $E_x(2_1^+)$ and $B(E2: 2_1^+ \rightarrow 0_1^+)$ values.

JMY, J Meng, P Ring, ZX Li, ZP Li & K Hagino, PRC 83, 014308 (2011)

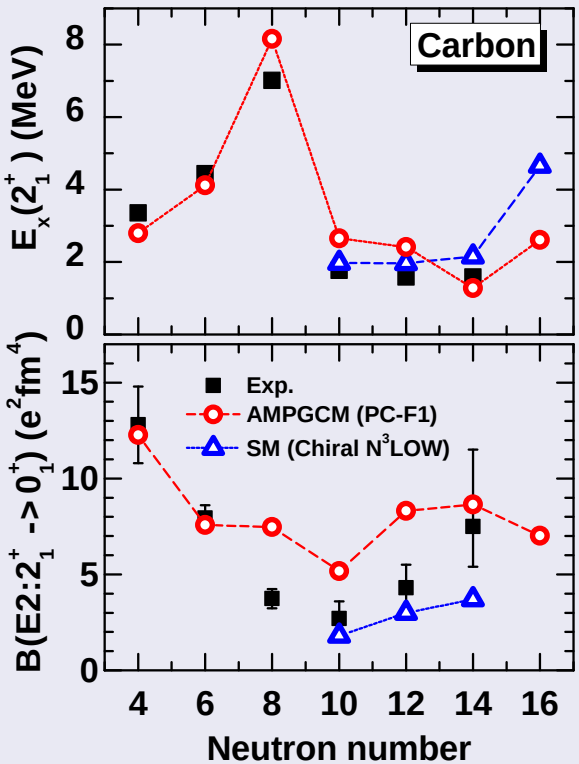

Figure: Excitation energies of 2_1^+ states $E_x(2_1^+)$ (MeV) and the $B(E2)$ values (e^2fm^4) for even-even carbon isotopes.

Carbon isotopes

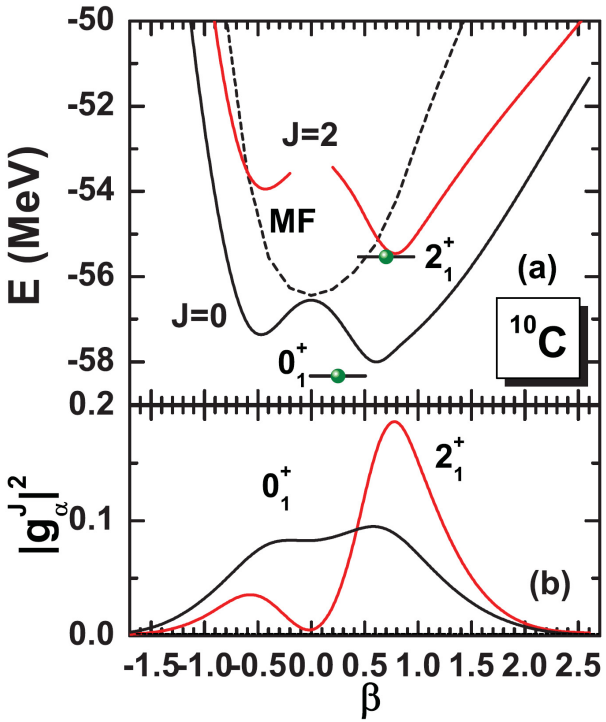

– Rather different $\langle\beta^2\rangle^{1/2}$ have been shown in ^{16,18,20}C, or even in ^{22}C

– Relative large $\langle\beta^2\rangle^{1/2}$ in ^{10,12,14}C are from large shape fluctuation.

JMY, J Meng, P Ring, ZX Li, ZP Li & K Hagino, PRC 83, 014308 (2011)

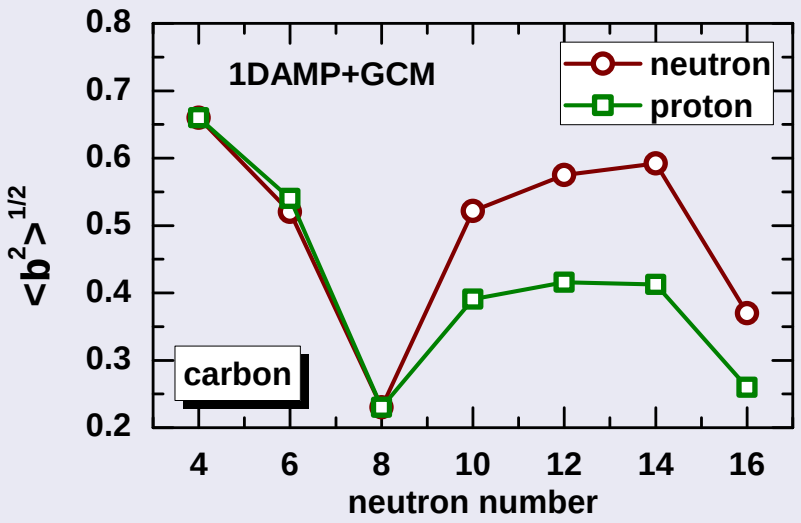

Figure: Average deformation of 0^+_1 state in the 1DAMP+GCM calculations for even-even carbon isotopes.

Potential energy surfaces in (β, γ) plane

Potential energy surfaces:

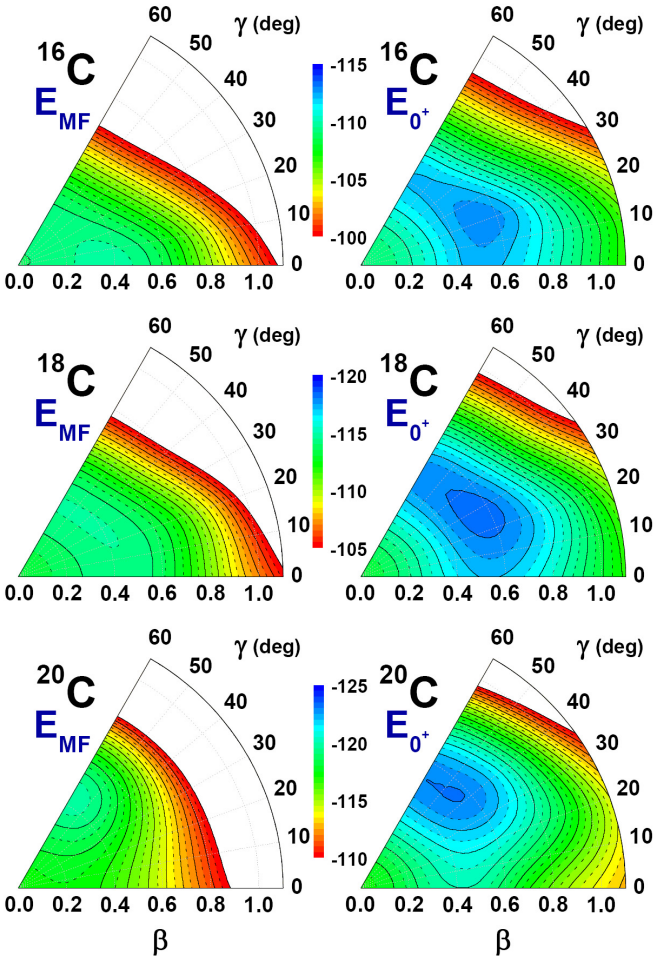

Probability distributions:

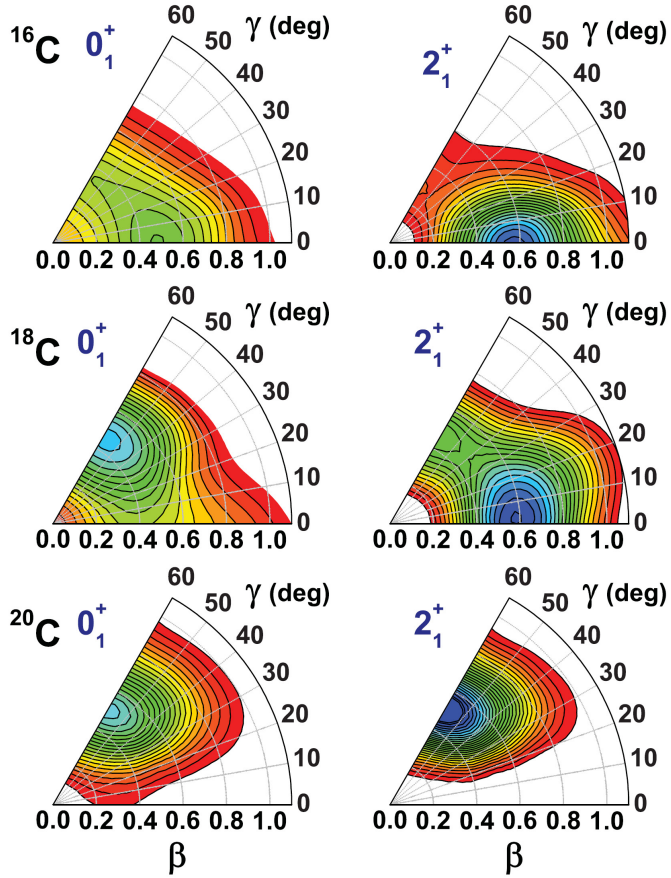

JMY, J Meng, P Ring, ZX Li, ZP Li & K Hagino, PRC 83, 014308 (2011)

Potential energy surfaces in (β, γ) plane

Potential energy surfaces:

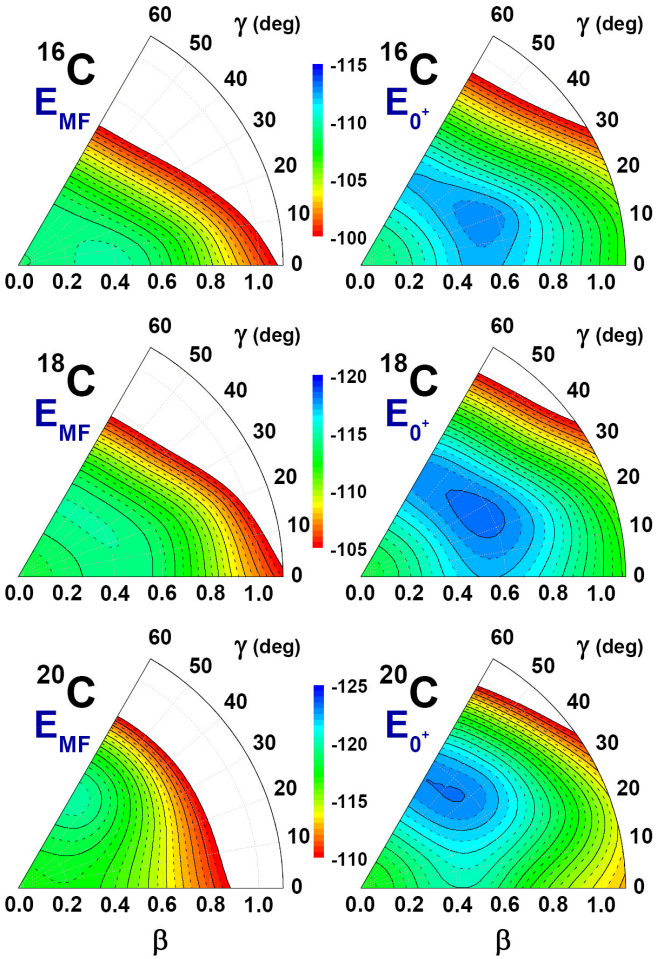

JMY, J Meng, P Ring, ZX Li, ZP Li & K Hagino, PRC 83, 014308 (2011)

Single-particle energy levels of neutrons in ^{16}C:

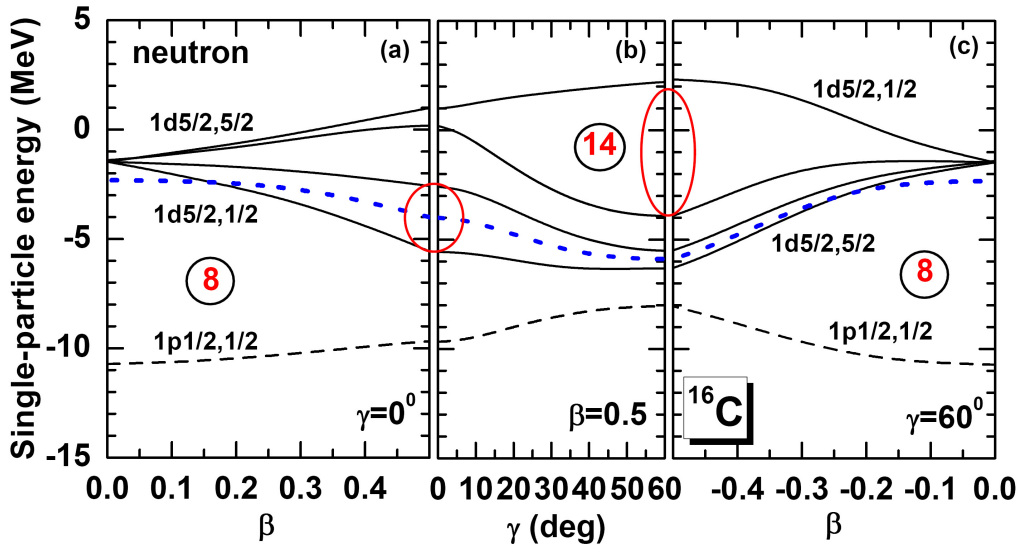

Effects of triaxiality in ^{16,18,20}C

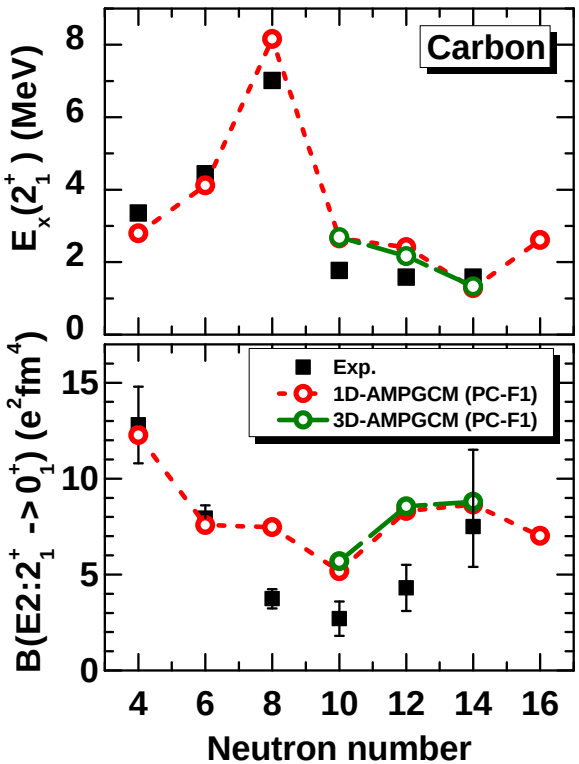

Figure: Excitation energies of 2_1^+ states $E_x(2_1^+)$ (MeV) and the $B(E2)$ values (e^2fm^4) for even-even carbon isotopes.

– **Even though there is an evident triaxial minimum on the projected PEC with $J = 0$ (^{18}C), the effect of triaxiality on the $E_x(2_1^+)$ and $B(E2 : 2_1^+ \rightarrow 0_1^+)$ is small.**

Outline

Summary and perspective

- A new parameter set PC-PK1 has been proposed:
  - Observables (binding energies, charge radii, and empirical pairing gaps) of 60 selected spherical nuclei (in fitting)
  - Saturation properties of nuclear matter and isospin dependence of binding energy
  - Properties of spherical and deformed nuclei (dynamic correlation energy is necessary)
- Based on the covariant EDF, angular momentum restored configuration mixing calculations have been realized by implementing the 3DAMP and GCM. The success of this MR-EDF calculations has been illustrated in both carbon and magnesium isotopes as well as in ^{80}Zr.
  - The effect of triaxiality is not evident for g.s (band) of concerned nuclei. (Is there any for other properties, nuclei?)
  - Much influence of pairing strength on ^{32}Mg.

Many things to be done ...

- NO particle number projection (to be implemented) (could be regularized!)
- Density-dependent terms in EDF (exponential form, which density?)
- ...

Collaboration

Relativistic EDF

Zhipan Li, Hua Mei	Southwest Univ. China
Zhao-Xi Li, Jiang Xiang	Southwest Univ. China (students)
Jie Meng, Peng-wei Zhao	Peking Univ. China
Peter Ring, Daniel Pena Arteaga	TUM, Germany
Dario Vretenar	Zagreb Univ. Croatia
Kouichi Hagino	Tohoku Univ. Japan

Non-relativistic EDF

Paul-Henri Heenen, Kouhei Washiyama	ULB, Belgium
Michael Bender	Université Bordeaux, France

Collaboration

Relativistic EDF

Zhipan Li, Hua Mei	Southwest Univ. China
Zhao-Xi Li, Jiang Xiang	Southwest Univ. China (students)
Jie Meng, Peng-wei Zhao	Peking Univ. China
Peter Ring, Daniel Pena Arteaga	TUM, Germany
Dario Vretenar	Zagreb Univ. Croatia
Kouichi Hagino	Tohoku Univ. Japan

Non-relativistic EDF

Paul-Henri Heenen, Kouhei Washiyama	ULB, Belgium
Michael Bender	Université Bordeaux, France

Center-of-Mass correction and average pairing gap

Center-of-Mass correction to total energy

As the translational symmetry is broken in mean-field approximation, the c.m. correction energy is calculated by the projection-after-variation in first-order approximation with the *posteriori* correction scheme,

$$E_{\mathrm{c.m.}}^{\mathrm{mic}} = -\frac{1}{2mA}\langle \hat{\mathbf{P}}_{\mathrm{c.m.}}^{2} \rangle, \tag{20}$$

with A mass number and $\hat{\mathbf{P}}_{\mathrm{c.m.}} = \sum_i^A \hat{\mathbf{p}}_i$ the total momentum in the c.m. frame. *M. Bender, K. Rutz, P.-G. Reinhard, and J. A. Maruhn, EPJA 7, 467 (2000)*

Average pairing gap

The pairing strength parameters V_τ can be adjusted by fitting the average pairing gaps to the experimental (five-point) odd-even mass difference,

$$\langle \Delta \rangle_\tau = \frac{\sum_k f_k u_k v_k < \Delta_\tau(\mathbf{r}) >_k}{\sum_k f_k u_k v_k}, \quad \Delta_\tau(\mathbf{r}) = \frac{\partial \mathcal{E}^{\mathrm{pair}}[\kappa, \kappa^*]}{\partial \kappa_\tau(\mathbf{r})}. \tag{21}$$

M. Bender, K. Rutz, P.-G. Reinhard, and J. A. Maruhn, EPJA 8, 59(2000)

Charge radii and neutron thickness

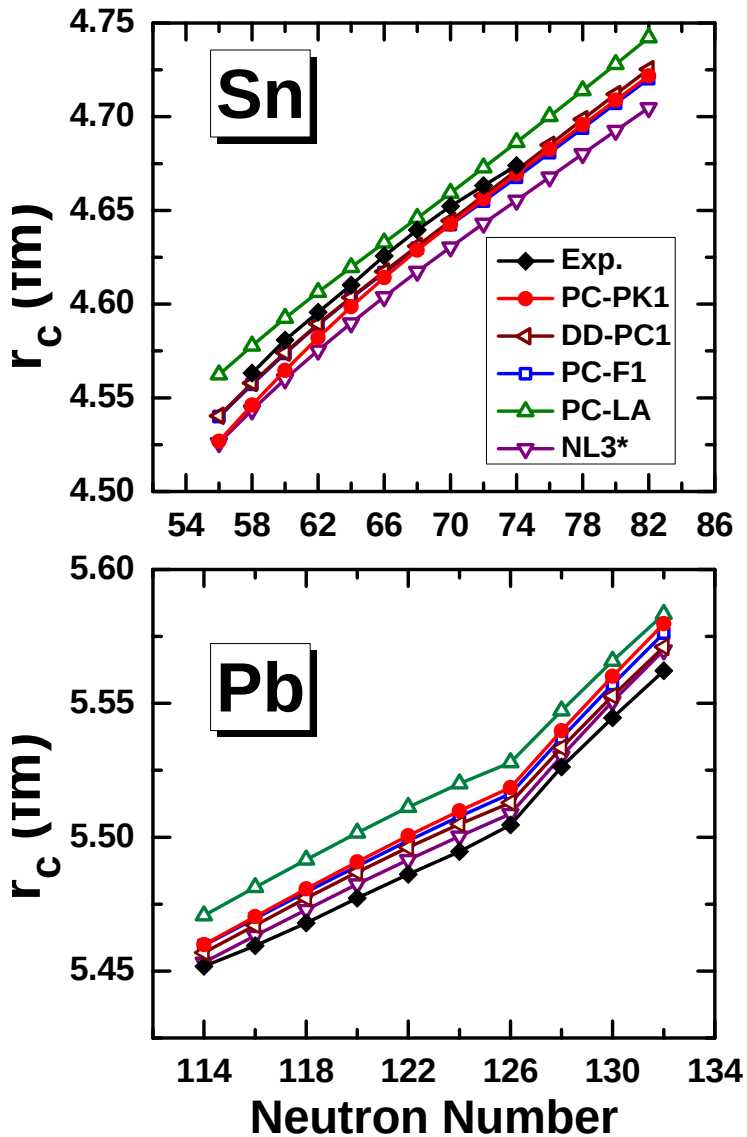

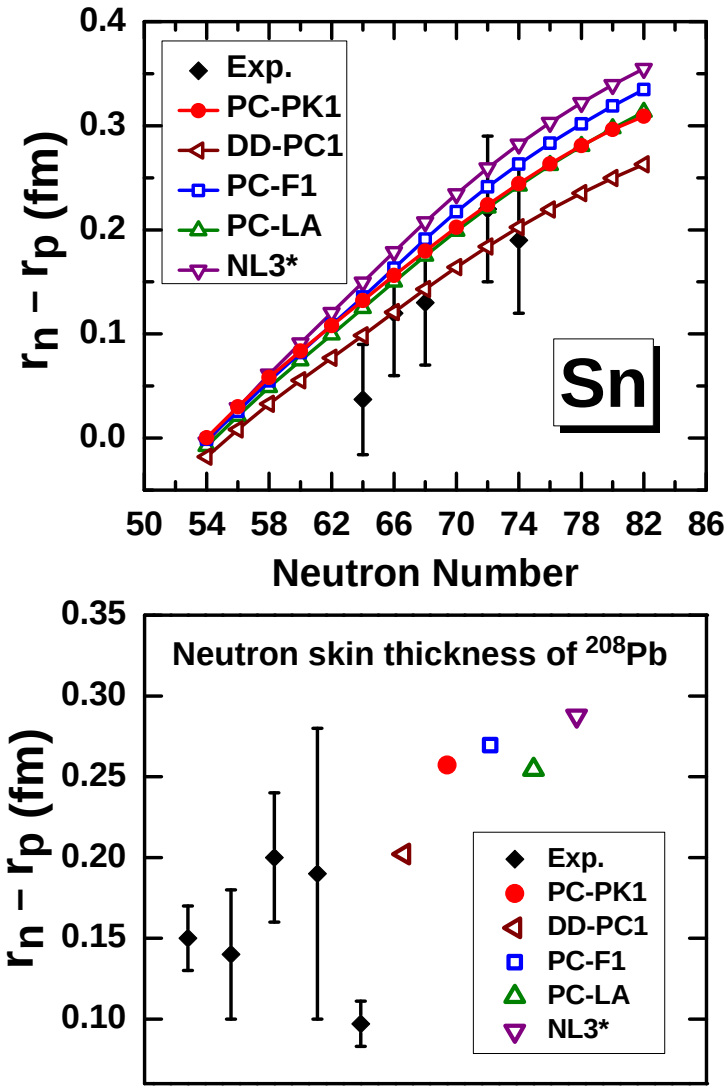

PW Zhao, ZP Li, JMY & J Meng, PRC82, 054319 (2010)

Fission barrier of ^{240}Pu

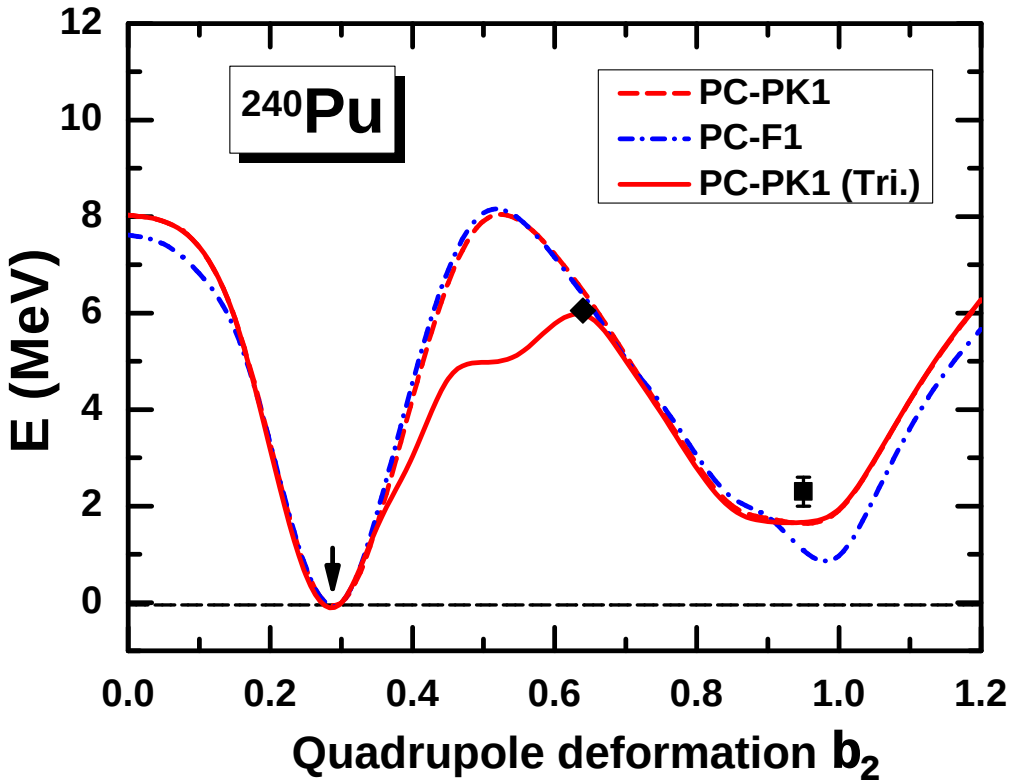

– The fission barrier and the excitation energy of the fission isomer are in agreement with the empirical values.

PW Zhao, ZP Li, JMY & J Meng, PRC82, 054319 (2010)

Neutron-rich Kr, Sr, Zr, and Mo isotopes

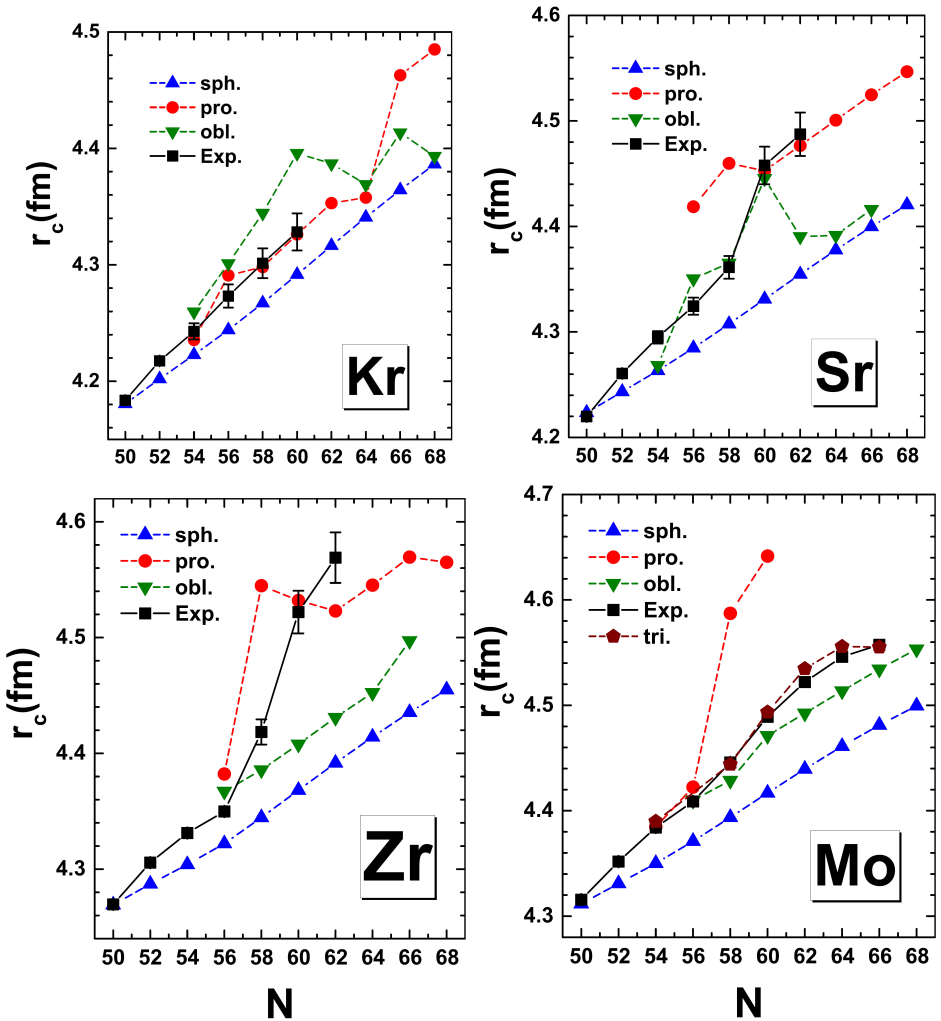

Figure: The charge radii of Kr, Sr, Zr, and Mo isotopes calculated with the PC-PK1 set together with a separable pairing force in Ref. *[Tian, Ma,& Ring, PLB676 (2009)44]*.

J Xiang, ZP Li, ZX Li, JMY & J Meng, arXiv:1107v1 [nucl-th] (2011)

Shape coexistence in ^{98}Sr and ^{100}Zr

Table: The $E_x(0_2^+)$ and $\rho^2(E0; 0_2^+ \rightarrow 0_1^+)$ of ^{98}Sr and ^{100}Zr, by the Bohr Hamiltonian calculations derived from the PC-PK1, in comparison between the data.

	^{98}Sr		^{100}Zr	
	Cal.	Exp.	Cal.	Exp.
$E_x(0_2^+)$(MeV)	0.216	0.215	0.468	0.331
$\rho^2(E0; 0_2^+ \rightarrow 0_1^+) \times 10^3$	116.841	51(5)	150.321	108(19)

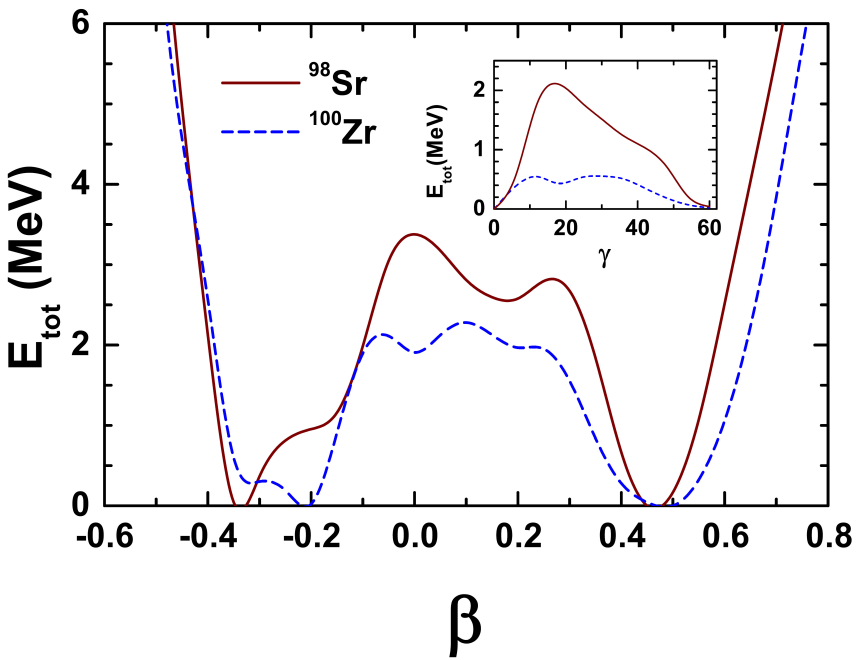

- The experimental data is reproduced rather well.
- The $\rho^2(E0)$ matrix element in ^{100}Zr is relative larger than that in ^{98}Sr, which is due to the relative lower barrier (along γ-direction) separating the competing prolate and oblate minima.

J Xiang, ZP Li, ZX Li, JMY & J Meng, arXiv:1107v1 [nucl-th] (2011)